Atomic Layer Deposition of Zirconium Oxide and Rare Earth Oxides from Heteroleptic Precursors

Sanni Seppälä

Department of Chemistry
Faculty of Science
University of Helsinki
Finland

DOCTORAL DISSERTATION

To be presented for public discussion with the permission of the Faculty of Science of the University of Helsinki, in Physicum Auditorium E204, Gustaf Hällströmin katu 2, on the 25th of October 2019 at 12 o'clock.

Helsinki 2019

Supervisor

Professor Mikko Ritala

Department of Chemistry

University of Helsinki

Helsinki, Finland

Reviewers

Professor Jaan Aarik

Institute of Physics

University of Tartu

Tartu, Estonia

Professor Mats Boman

Department of Chemistry

Uppsala University

Uppsala, Sweden

Opponent

Professor Sami Franssila

Department of Chemistry and Materials Science

Aalto University

Espoo, Finland

ISBN 978-951-51-5524-5 (paperback)
ISBN 978-951-51-5525-2 (PDF)
http://ethesis.helsinki.fi/

Unigrafia
Helsinki 2019

Abstract

This thesis focuses on the development of new atomic layer deposition processes for zirconium oxide and rare earth oxides. Atomic layer deposition (ALD) is a chemical thin film deposition method that is capable of generating films with excellent properties including conformality, uniformity, high density and pinhole free structure. Because of these film properties, ALD has become the best and often the only method capable of fulfilling the demands of many applications, microelectronics being the best example. The unique properties of ALD films are enabled by the self-limiting growth mechanism of these films.

Traditionally, ALD metal precursors have been homoleptic, meaning that the compound contains only one type of ligands. In the search of precursors with higher thermal stability, growth rate and uniformity, heteroleptic precursors with more than one type of ligands have gained interest. However, properties of different ligand combinations are hard to predict which means that comprehensive studies on the precursors with different oxygen sources are needed.

In this work, heteroleptic precursors for rare earth oxides and zirconium oxide were studied. ZrO_2 and rare earth oxides are so called high-κ materials with a wide variety of applications ranging from microelectronics to fuel cells, optics and catalysis. For the ALD of ZrO_2, three metal precursors, Zr(Me_5Cp)(TEA), Zr(MeCp)(TMEA) and ZrCp(^{t}BuDAD)(O^{i}Pr) were evaluated with water or ozone as the oxygen source. Self-limiting growth processes typical for ALD were found for two Zr precursors with ozone. The deposition temperature for the self-limiting Zr(Me_5Cp)(TEA)/O_3 process was as high as 375 °C making Zr(Me_5Cp)(TEA) one of the most thermally stable precursors for zirconium. ZrO_2 films with high purity were deposited with the three precursors especially when ozone was used as the oxygen source.

Heteroleptic cyclopentadiene-amidinate precursors RE(^{i}PrCp)(^{i}Pramd) were studied for Y, La, Pr, Gd and Dy. Water and ozone were studied as oxygen sources. In addition to these common oxygen sources, also ethanol as well as water and ozone in the same deposition process separated by a purge period were tested for the La_2O_3 deposition. Self-limiting growth was confirmed for Y_2O_3, La_2O_3 and Gd_2O_3.

Preface

The research and experimental work for this thesis work were conducted at the University of Helsinki in the Laboratory of Inorganic Chemistry.

Professors Markku Leskelä and Mikko Ritala are greatly thanked for the opportunity to work in their group for all these years. I would have never guessed during my first summer job in the field of chemistry as a bachelor student in 2010 that I would one day write a PhD thesis. Thank you for all your advice and guidance during these years.

The reviewers of this thesis, Professor Jaan Aarik and Professor Mats Boman are thanked for their helpful comments.

I wish to thank my coauthors for their collaboration. Thank you D.Sc. (Tech.) Jaakko Niinistö for the help and advice, Dr. Timothee Blanquart and Mr. Mikko Kaipio for the help with the experimental work regarding Y_2O_3 and Dy_2O_3 and Dr. Kenichiro Mizohata and Professor Jyrki Räisänen for the TOF-ERDA measurements that were not always that straight forward. Thank you Dr. Marko Vehkamäki for the help with the electrical measurements and Mr. Miika Mattinen for the AFM measurements. Special thanks is given for Air Liquide Laboratories and especially my coauthors Dr. Clement Lansalot-Matras and Dr. Wontae Noh for the fruitful collaboration that enabled this work to be done.

Thank you also for all the co-workers in the lab for making every day at work interesting and often fun. Mr. Mikko Heikkilä, Dr. Marianna Kemell and Dr. Peter King are additionally thanked for their help with XRD and XRR, FESEM and EDX and Raman spectroscopy. Special thanks goes to Ms. Katja Väyrynen and Dr. Jani Holopainen for their support and great sense of humor also outside the working hours.

The research leading to this thesis received funding from the Academy of Finland (Finnish Centre of Excellence in Atomic Layer Deposition).

I want to thank my family and friends for their support and especially my husband Matti, without whom this thesis would never have finished. Thank you for always pushing me forward, especially over the last year of big changes.

Karlstein am Main, September 2019

Sanni Seppälä

Table of Contents

Abstract ... 3

Preface ... 4

List of original publications ... 7

Abbreviations ... 8

1 Introduction ... 9

2 Atomic layer deposition ... 10

2.1 Principles of ALD ... 10

2.2 ALD precursors ... 12

2.2.1 Precursor requirements ... 12

2.2.2 Metal precursors ... 13

2.2.3 Oxygen precursors ... 15

3 Rare earth oxide thin films ... 18

3.1 Properties of rare earth oxides ... 18

3.2 Atomic layer deposition of rare earth oxides ... 19

4 Zirconium dioxide thin films ... 25

4.1 Properties of zirconium dioxide ... 25

4.2 Atomic layer deposition of zirconium dioxide ... 26

5 Applications of rare earth and zirconium oxide thin films ... 30

5.1 Microelectronics ... 30

5.1.1 MOSFET ... 30

5.1.2 Memory devices ... 32

5.2 Solid oxide fuel cells ... 33

6 Experimental section ... 35

6.1 Precursors ... 35

6.2 Film depositions ... 35

6.3 Characterization of the films ... 36

7 Results and discussion ... 38

7.1 Precursor properties ... 38

7.2 Rare earth oxide depositions ... 40

7.2.1 La_2O_3 [II] ... 40

7.2.2 PrO_x [I, IV] ... 44

7.2.3 Gd_2O_3 [I, IV] ... 45

7.2.4 Y_2O_3 [I, IV] ... 46

7.2.5 Dy_2O_3 [I] ... 47

7.2.6 Summary on the RE oxide studies 47
7.3 Zirconium oxide depositions [III] 49
7.3.1 Zr(Me_5Cp)(TEA) 49
7.3.2 Zr(Cp)(^{t}BuDAD)(O^iPr) 52
7.3.3 Zr(MeCp)(TMEA) 54
7.3.4 Summary of the ZrO_2 studies 56
8 Conclusions 57
9 References 58

List of original publications

This doctoral dissertation is based on the following publications, which in the text are referred to by their Roman numerals.

I Seppälä, S.; Niinistö, J.; Blanquart, T.; Kaipio, M.; Mizohata, K.; Räisänen, J.; Lansalot-Matras, C.; Noh, W.; Ritala, M.; Leskelä, M. Heteroleptic Cyclopentadienyl-Amidinate Precursors for Atomic Layer Deposition (ALD) of Y, Pr, Gd, and Dy Oxide Thin Films. *Chem. Mater.* **28** (2016) 5440 – 5449.

The author made the deposition experiments and performed the thickness and crystallinity analyses for Gd_2O_3 and PrO_x and partly for Y_2O_3 and Dy_2O_3 and took all the FESEM images. The author wrote the first draft and finalized the paper together with the co-authors.

II Seppälä, S.; Niinistö, J.; Mattinen, M; Mizohata, K.; Räisänen, J.; Noh, W.; Ritala, M.; Leskelä, M. Atomic Layer Deposition of Lanthanum Oxide with Heteroleptic Cyclopentadienyl-Amidinate Lanthanum Precursor - Effect of the Oxygen Source on the Film Growth and Properties. *Thin Solid Films* **660** (2018) 199 – 206.

The author made the deposition and annealing experiments and performed the thickness and crystallinity analyses. The author wrote the first draft and finalized the paper together with the co-authors.

III Seppälä, S.; Vehkamäki, M.; Mizohata, K.; Räisänen, J.; Noh, W.; Ritala, M.: Leskelä, M. Comparative Study on the Use of Novel Heteroleptic Cyclopentadienyl-based Zirconium Precursors with H_2O and O_3 for Atomic Layer Deposition of ZrO_2. *J. Vac. Sci. Tech. A* **37** (2019) 020912.

The author made the deposition experiments and performed the thickness and crystallinity analyses. The author made the electrical measurements together with M.V. The author wrote the first draft and finalized the paper together with the co-authors.

IV Niinistö, J.; Blanquart, T.; Seppälä, S.; Ritala, M.; Leskelä, M. Heteroleptic Precursors for Atomic Layer Deposition. *ECS Transactions **64*** (2014) 221 – 232.

The author made the deposition experiments and performed the thickness and crystallinity analyses for Gd_2O_3 and PrO_x. The author participated in the finalizing of the paper that was mostly written by J.N.

Abbreviations

AFM	Atomic force microscopy
ALD	Atomic layer deposition
amd	Amidinate, NR(CR´)NR
CHT	Cycloheptatrienyl, C_7H_{14}
Cp	Cyclopentadienyl, C_5H_5
CMOS	Complementary metal-oxide-semiconductor
CVD	Chemical vapor deposition
dmae	Dimethylaminoethoxide, $OC_2H_5N(CH_3)_2$
dmb	2,3-dimethyl-2-butoxy, $OC(CH_3)_2CH(CH_3)$
DPDMG	N,N′-diisopropyl-2-dimethylamido-guanidinate, $(^iPrN)_2CN(CH_3)_2$
DRAM	Dynamic random access memory
Me_2pz	3,5-dimethylpyrazolate
MOSFET	Metal-oxide-semiconductor field effect transistor
PEALD	Plasma enhanced atomic layer deposition
RE	Rare earth
ReRAM	Resistive switching random access memory
SOFC	Solid oxide fuel cell
^tBu	tert-butyl
thd	Tris(2,2,6,6-tetramethyl-3,5-heptanedionato)
XRD	X-ray diffraction
XRR	X-ray reflection

1 Introduction

Today, we live in a world full of technology. In order to make faster and more powerful electronic devices, the size of the components is shrinking, and new materials and designs are sought. The fast down-scaling of the microelectronic components has led to a situation where new materials are needed to maintain the pace of improvement. Atomic layer deposition (ALD) has become the number one method to produce high quality films for microelectronics. In fact, ALD is the only method that can enable the production at the nanoscale on demanding structures with precise thickness control as well as film conformality and uniformity.

Zirconium oxide and rare earth oxides are so called high-κ oxides. High-κ material refers to a compound with a high dielectric constant, also called relative permittivity, ε_r. Permittivity is related to the capability of a material to resist applied electric field. The relative permittivity of vacuum is 1.0. In microelectronics, a material is considered to have high dielectric constant if it is higher than the dielectric constant of SiO_2 which is 3.9. For example, Al_2O_3 is already a high-κ material with a dielectric constant of around 9.

Zirconia and rare earth oxides are amongst the promising materials for microelectronics, but they are very versatile materials with applications in many other areas as well, such as in fuel cells, catalysis and optics. In the recent years, the research focus has shifted from precursors and ALD process development more towards application development and only a few new metal precursors for Zr and RE elements have been reported lately. However, to answer the demanding expectations set for the future high-κ materials, multicomponent materials are increasingly studied. These materials include doped, ternary and quaternary compounds. With ALD, the complex compounds can be deposited by simply combining binary processes. Film composition can be tuned by varying the ALD cycle ratios of the binaries. The main requirement is that the binary processes have a common deposition temperature. This can be assured by developing ALD processes having wide deposition temperature range. For this, basic studies on precursors and processes are the key.

In this thesis work, atomic layer deposition processes were developed for zirconium and rare earth oxide materials from new heteroleptic precursors and the properties of the deposited films were studied. Heteroleptic compounds have at least two different types of ligands and they are used in an effort to combine the best properties of the parent homoleptic precursors to improve for example film purity and thermal stability of the precursors. The end result is often unpredictable, however, highlighting the importance of precursor development and process studies.

This thesis comprises four papers that study new precursors for the ALD of rare earth and zirconium oxides. The principles of ALD are introduced in Chapter 2, together with the requirements for ALD precursors and the different types of metal and oxygen precursors used in ALD. Chapters 3 and 4 focus on the properties and ALD processes of rare earth oxides and zirconium oxide. Some applications for these materials are introduced in Chapter 5. The experimental procedures related to papers I – IV are described in Chapter 6 and the results are summarized in Chapter 7. Conclusions of the work are collected in Chapter 8.

2 Atomic layer deposition

2.1 Principles of ALD

Atomic layer deposition (formerly called atomic layer epitaxy, ALE) was invented in Finland in the 1970s to manufacture thin film electroluminescent (TFEL) displays.[1] ALD is a chemical deposition method based on alternating pulses of precursors separated from each other with purging periods. This ensures that the reactions occur only on the surface of a substrate with molecules adsorbed during the previous precursor pulse while all the precursors in the gas phase are purged away. There is only a certain number of active reaction sites on the surface meaning that when these have reacted, no more film can be formed. Because of this, the film growth in ALD is self-limiting and the film thickness is dependent only on the number of the deposition cycles.[2] The by-products and unreacted precursor molecules are purged away before the next pulse. In this way conformal, uniform and pinhole free films can be deposited.[3] Also the film composition can be easily tuned by varying cycle ratios of the different components.[4,5]

One deposition cycle in ALD of binary metal oxides consists of four steps: pulse of the first precursor, purge, pulse of the second precursor, and purge (Figure 1). In the first step, the substrate is exposed to the gaseous precursor and the precursor is chemisorbed on the substrate surface. In the second step, the unreacted precursor molecules are purged away by an inert gas. In the third step, the second precursor is transported to the substrate and a reaction the surface species formed by the first precursor takes place. In the fourth step the excess of the second precursor molecules and the reaction byproducts are purged away.[6] The self-limiting growth that is the key feature of ALD means that increasing the pulse length does not affect the growth rate, but it stays constant. If the precursor is decomposing, increasing pulse length leads to an increased growth rate. If the precursor is etching the already formed film, the growth rate is decreased from the self-limiting value (Figure 2).

In ALD the film grows on all surfaces exposed to the precursor. This means that ALD is an excellent method for coating high aspect ratio substrates. Substrate materials can vary from glass to polymers and from wafers to particles or nanotubes.[7] The slowness of the film deposition is considered as the biggest drawback of ALD. However, in many applications the film thicknesses are in the range of nanometers and the slow growth time is not a problem for these applications. Also, the film quality achieved with ALD is superior to many other thin film methods making ALD the only practical way to deposit films for some demanding applications such as microelectronics.

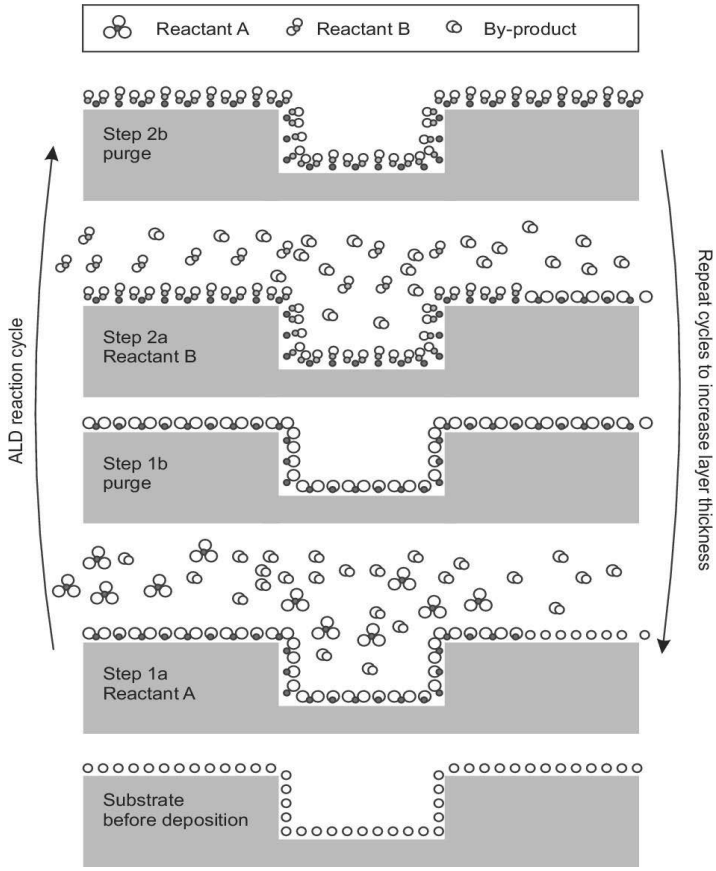

Figure 1. Illustration of one ALD cycle. Reprinted from *J. Appl. Phys*. 113, **2013**, 021301, V. Miikkulainen et al. with the permission of AIP Publishing.

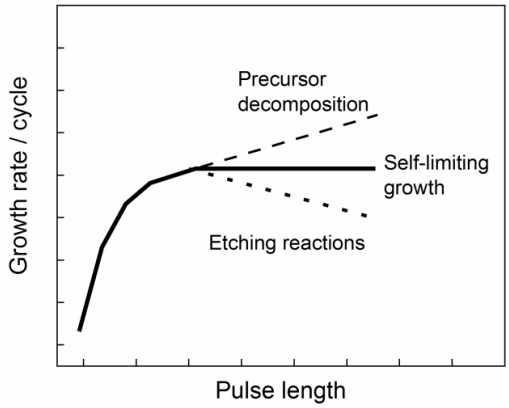

Figure 2. Self-limiting film growth is achieved when the growth rate does not change with increasing precursor pulse length. Constantly increasing growth rate may be caused by precursor decomposition and decreasing growth rate by etching reactions.

For a given ALD process, there is a suitable temperature range that depends on the precursor properties. Figure 3 depicts the mechanisms that can affect the growth rate at different temperatures. If the temperature is too low, there might be precursor condensation that increases the growth rate above the self-limiting growth rate (b), or too low reactivity of the precursors causing decreased growth rate (c). On the other hand, if the temperature is too high, the precursor might decompose increasing the growth rate (d) or desorb from the surface decreasing the growth rate compared to the self-limiting conditions (e). In the correct deposition temperature range where the self-limiting growth occurs, the growth rate may be constant (a), or dependent on the process temperature (f). The temperature range where the growth rate is independent of the temperature is often called as an ALD window. However, it is not a prerequisite for an ALD process.[2] More important is that the growth is self-limiting.

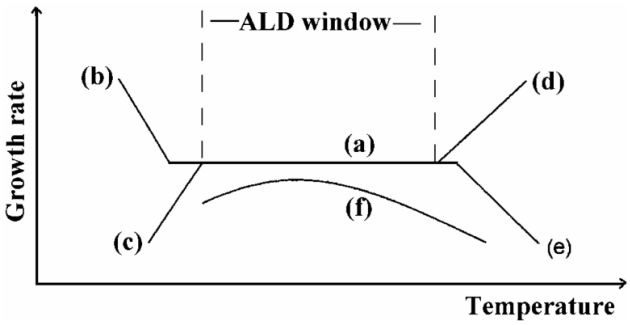

Figure 3. Scheme of (a) an ALD processing window limited by (b) precursor condensation, (c) insufficient reactivity, (d) precursor decomposition and (e) precursor desorption. If the deposition rate is dependent on the temperature dependent number of available reactive sites as in (f), actual ALD window cannot be observed. Reprinted from Ref. 6, with permission from WILEY-VCH Verlag GmbH & Co. KGaA, Weinheim (2004).

2.2 ALD precursors

2.2.1 Precursor requirements

For successful ALD precursors, there are many requirements from which some are essential and the others good to have but not necessary (Table 1). In ALD, gaseous precursors are transported to the substrate meaning that the precursors need to be volatile. The reactions should be fast and complete to ensure fast growth, high film purity and efficient usage of the precursors. The precursor should not decompose by itself or dissolve into the substrate because these destroy the self-limiting growth which is the key feature of ALD. There should not be etching of the film or substrate and the precursors should be of sufficient purity, which depends on the process and application. The desirable properties include unreactive volatile byproducts to avoid corrosion and decrease of the growth rate by readsorption or etching reactions, easiness of synthesis and handling, nontoxicity and environmental friendliness as well as affordable price.[3,IV]

Table 1. ALD precursor requirements [IV]

Necessary properties	Desirable but not necessary
Volatility	Unreactive volatile byproducts
Fast and complete reactions	Easiness in synthesis and handling
No self-decomposition	Nontoxic and environmentally friendly
No etching of the film or substrate material	Inexpensive
Sufficient purity	
No dissolution into the film substrate	

2.2.2 Metal precursors

In ALD, the precursor can affect for example the purity and crystal phase of the films, making it of utmost importance to study different precursors to develop a process with the best properties for the chosen application. Options for the oxygen source are more limited than for the metal precursors, but in many cases the oxygen source has been shown to have a tremendous effect on the properties such as purity of the metal oxide films.

A variety of different kinds of metal compounds have been studied as ALD precursors. The diverse ligand types used in the metal precursors are shown in Figure 4. Some examples of the different ligand families are introduced in this chapter.

Metal halides are examples of inorganic metal precursors. They often have high thermal stability, but the byproducts are corrosive. These byproducts have been proposed to decrease film growth by poisoning the reactive sites or by etching the already grown film.[8,9] In the etching, hydrogen halide byproduct reacts with the metal oxide film forming volatile metal halide or metal oxyhalide that is then purged away. Etching can also be caused by the precursor itself, like in the case of the $NbCl_5/H_2O$ process: in a reaction between $NbCl_5$ and Nb_2O_5 film, a volatile $NbOCl_3$ is formed causing highly nonuniform and irreproducible film growth.[10,11] In the poisoning reaction the number of reactive sites on the film surface is decreased. For example, HCl is formed in the reaction between a metal chloride and water, and can react with the -OH groups on the surface of the film releasing water and leaving the surface Cl-terminated.[8] Another drawback of the solid metal chloride precursors has been observed with the $ZrCl_4/H_2O$ process where very fine precursor particles are transported by the carrier gas to the substrate and incorporated in the film.[3]

Metal alkoxides and β-diketonates are examples of precursors with metal-oxygen bonds. Alkoxide ligands bond to the metal via one O atom and β-diketonates via two oxygen atoms. Alkoxide precursors tend to form oligomers because the ligands do not screen the metal atoms from other species nearby. For sufficient volatility, bulky alkoxide ligands with better screening property are often needed.[12] The thd ligand, tris(2,2,6,6-tetramethyl-3,5-heptanedionato), that belongs to the β-diketonate group has been particularly important in the development of ALD processes for lanthanide oxides.[13] Lanthanide ions are large and need high coordination numbers to satisfy their coordination spheres. The synthesis of the $RE(thd)_x$ chelates was first published by Eisentraut and Sievers in 1965.[14]

Organometallic precursors have direct metal-carbon bonds. Cyclopentadienyl (Cp) and alkyl precursors belong to this group. Properties of the Cp precursors can easily be tuned by changing the substituents in the Cp ring which makes them very versatile ligands. Cyclopentadienyls are good electron donors and form stable bonds with metals which ensures reasonable thermal stability of the compounds.[12] However, the bulky Cp can decrease the growth rate. The best known and very widely used metal alkyl precursor is trimethylaluminum which, when used with water, is the textbook example of an ALD process.[8]

Examples of precursors with metal-nitrogen bonds are amides, amidinates and guanidinates. These precursors do not have a direct metal to carbon bond which might help decreasing carbon contamination in the films. In an analogy to the alkoxides and β-diketonates, alkylamide ligands bond to metal atoms via one nitrogen atom and amidinates and guanidinates via two nitrogen atoms. Alkylamide ligands effectively prevent interactions between neighboring molecules thus leading to high volatility. Amidinates have high thermal stability because of the chelating effect.[12]

Traditionally, ALD metal precursors have been homoleptic, meaning that all the ligands in the molecule are similar to each other. An example of a homoleptic precursor is $ZrCl_4$. Heteroleptic precursors have at least two different kinds of ligands, for example $CpZr(NMe_2)_3$ is a heteroleptic Zr precursor. The aim of the heteroleptic approach is to combine the best properties of the parent homoleptic compounds. Desired properties include improved thermal stability, growth rate and volatility. However, it is hard to predict the outcome of the different ligand combinations and therefore they need to be studied experimentally. In the past ten years, more and more heteroleptic precursors have been reported in ALD. The reason is apparently the ever-increasing requirements for materials in the future microelectronic industry, which drives the development of many materials, and not least the high-κ dielectrics.

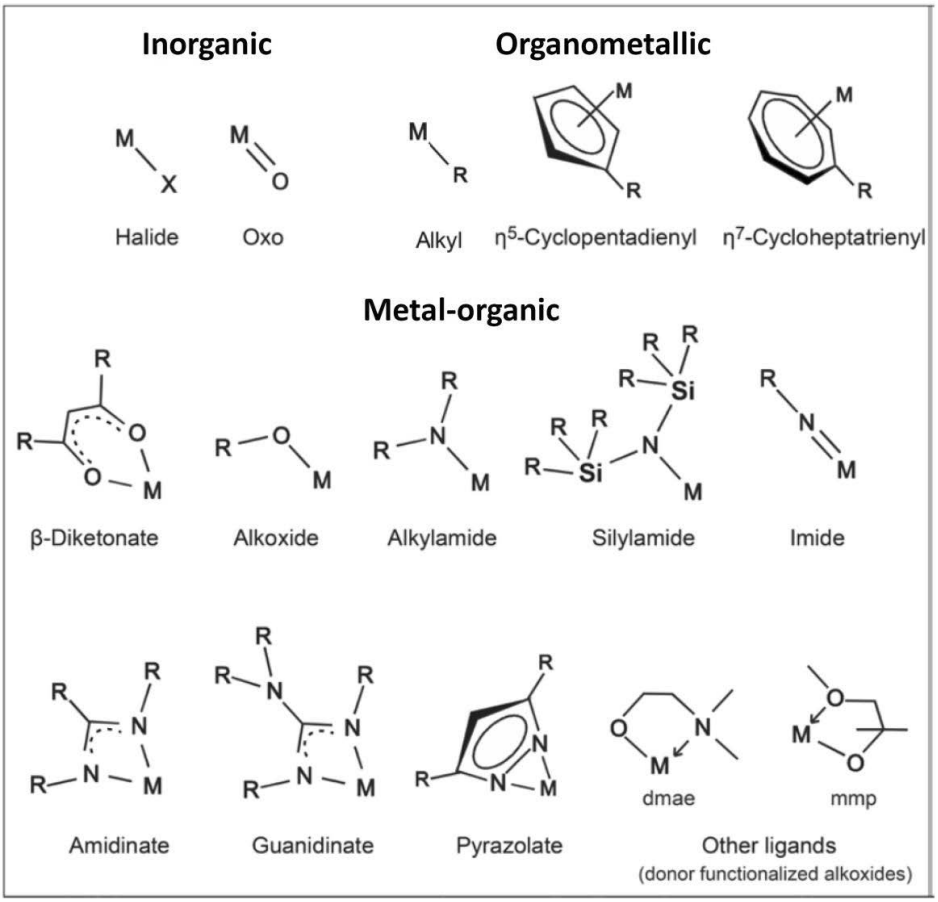

Figure 4. Examples of the types of ligands used in ALD metal precursors.[IV]

2.2.3 Oxygen precursors

Many oxygen sources have been studied for the deposition of metal oxides by ALD. The oxygen source can affect dramatically the film properties and by changing the oxygen source it is possible for example to tune the oxidation state of the metal or crystalline phase of the films.[15] The most popular oxygen source is water which has many advantages such as user and environment friendliness. However, some materials, like RE oxides, are hygroscopic which means that they absorb water. Long purge times are needed to ensure self-limiting growth, but this approach is not always applicable in industrial processes.

Aqueous solution of H_2O_2 has also been studied as an oxygen source in ALD. H_2O_2 is more reactive than water and the idea is that it could improve film properties compared to water. Higher growth rate compared to water has been reported for example in In_2O_3 deposition.[16] In the case of ZrO_2, growth mechanism and phase composition did not depend on the oxygen source,[17] but lower permittivity and leakage current have been reported for the films deposited with the H_2O_2-H_2O solution as the oxygen source compared to water.[18]

Some metal precursors have low reactivity towards water and need stronger oxidizer such as ozone or oxygen plasma. The $RE(thd)_x$ compounds are a good example of precursors having low reactivity towards water. They are usually used together with ozone. Although ozone can be very useful for ALD especially in those cases when water is not a good option, it has its own drawbacks. Because ozone is a strong oxidizer, it can oxidize also the substrate leading to undesirable interface layers. In microelectronic applications this can be detrimental as it decreases the total capacitance of the dielectric stack. Ozone is not very stable molecule and some substrate materials can catalyze its decomposition which might cause nonuniformity to the film especially in cross-flow reactors and in trenches and other high aspect ratio substrates.[5] Also, carbonate formation has been observed when ozone has been used to deposit metal oxides prone to carbonate formation, such as lanthanum oxide and calcium oxide.[19,20] On the other hand, efficient ligand removal by combustion with ozone can lead to increased film purity compared to water.[21,III]

Several milder oxygen sources have been studied to avoid the interfacial layer formation between an oxide film and silicon substrate. These include carboxylic acids, alcohols, N_2O and O_2. Molecular oxygen is usually not reactive, but it has been used for example in the deposition of very thin ZrO_2 and La_2O_3 films (3 – 6 nm) with lanthanum tris(N,N′-diisopropylformamidinate) and zirconium tetrakis(diethylamine).[22,23] Jeong et al.[24] compared H_2O, O_2 and N_2O as oxygen sources in the deposition of ZrO_2. The zirconium source was tert-butoxide. With water, crystalline films were deposited at 170 °C whereas with O_2 and N_2O amorphous films were deposited. The interfacial layer between the film and Si substrate was slightly thinner when O_2 or N_2O were used compared to H_2O.[24]

From alcohols, for example methanol, ethanol and isopropanol have been studied as oxygen sources in ALD. Aluminum oxide has been deposited from TMA and isopropanol successfully without interface layer formation at 350 °C on GaAs [25] and at 250 °C on Si substrates.[26] The growth rate at 350 °C on GaAs was 0.8 Å/cycle which is slightly lower than with water (1.0 Å/cycle).[25] Marstell and Strandwitz have reported clearly higher carbon content in films deposited with isopropanol compared to water.[27] In this thesis work, ethanol was studied as an oxygen source in the deposition of La_2O_3. It was noted that at a higher deposition temperature of 300 °C the growth rate increased significantly compared to lower temperatures. This was attributed to the water formation through dehydration of ethanol release during the deposition (see Chapter 7.2.1).[II]

Another way to avoid the interlayer formation in ALD is to use reactions between carboxylic acid and metal alkoxide.[28] Carboxylic acids have low oxidation power and the film is formed via surface esterification.[29] Yet another approach that has been studied to deposit metal oxide films without interface layer is to use metal alkoxides as both metal and oxygen sources.[30,31,32] The other precursor is a metal halide and the metal oxide is formed via an alkyl halide elimination. Metal alkyl precursors can also be used instead of halides.[30] The metal can be the same in both precursors to form binary oxides or different so that mixed metal oxide films are obtained. For example, $Al_xZr_yO_z$ has been deposited this way from $Al(OEt)_3$ and $ZrCl_4$ and $Zr_xTi_yO_z$ from $Ti(O^iPr)_4$ and $ZrCl_4$.[30,33]

This thesis work is focused on thermal ALD, but metal oxide films can also be deposited with plasma enhanced atomic layer deposition (PEALD). The advantage of PEALD is enhanced reactivity compared to the thermal ALD, especially at low deposition temperatures, which enables the use of temperature-sensitive substrates and metal precursors with low reactivity for example towards water. As a down side, the step coverage on high aspect ratio structures is often observed to be decreased with PEALD compared to the thermal ALD.[34,35] Plasma enhanced ALD cannot be applied in batch processing of large number of substrates. Oxygen plasma is commonly used as an oxygen source in PEALD. The main reactive species in oxygen plasma are oxygen radicals. Due to the high reactivity of the oxygen plasma, interfacial oxide layer formation similar to the thermal ALD using ozone has been reported with PEALD.[35]

3 Rare earth oxide thin films

3.1 Properties of rare earth oxides

Rare earth oxides refer to the oxides formed by scandium (atomic number 21), yttrium (39) and lanthanide metals (from lanthanum to lutetium, atomic numbers 57 - 71) (Figure 5). In the solid state, the stable oxidation state for rare earths is +3, and thus they are forming sesquioxides with a formula RE_2O_3. Ce, Pr and Tb are also stable at +4 oxidation state and Eu at +2 oxidation state.[36]

The ionic radius of the lanthanide Ln^{3+} ions decreases when moving from left to right along the series. This is caused by poor screening of the electrons on the 4f orbitals. Therefore, the effective nuclear charge experienced by the outer electrons increases with increasing atomic number, the electrons are pulled closer to the nucleus and the radius decreases.[37] The decrease of the radius is called lanthanide contraction. The effective radius of the La^{3+} ion is 103.2 pm and Lu^{3+} 86.1 pm. In comparison, the effective radius of the Sc^{3+} ion is 74.5 pm and Y^{3+} 90 pm.[38]

1 H																	2 He
3 Li	4 Be											5 B	6 C	7 N	8 O	9 F	10 Ne
11 Na	12 Mg											13 Al	14 Si	15 P	16 S	17 Cl	18 Ar
19 K	20 Ca	21 Sc	22 Ti	23 V	24 Cr	25 Mn	26 Fe	27 Co	28 Ni	29 Cu	30 Zn	31 Ga	32 Ge	33 As	34 Se	35 Br	36 Kr
37 Rb	38 Sr	39 Y	40 Zr	41 Nb	42 Mo	43 Tc	44 Ru	45 Rh	46 Pd	47 Ag	48 Cd	49 In	50 Sn	51 Sb	52 Te	53 I	54 Xe
55 Cs	56 Ba	57 La*	72 Hf	73 Ta	74 W	75 Re	76 Os	77 Ir	78 Pt	79 Au	80 H g	81 Tl	82 Pb	83 Bi	84 Po	85 At	86 Rn
87 Fr	88 Ra	89 Ac**	104 Rf	105 Db	106 Sg	107 Bh	108 Hs	109 Mt	110 Ds	111 Rg	112 Cn	113 Nh	114 Fl	115 Mc	116 Lv	117 Ts	118 Og

Lanthanides*	58 Ce	59 Pr	60 Nd	61 Pm	62 Sm	63 Eu	64 Gd	65 Tb	66 Dy	67 Ho	68 Er	69 Tm	70 Yb	71 Lu
Actinides**	90 Th	91 Pa	92 U	93 Np	94 Pu	95 Am	96 Cm	97 Bk	98 Cf	99 Es	100 Fm	101 Md	102 No	103 Lr

Figure 5. Periodic table of the elements. The rare earth metals and zirconium are highlighted.

Rare earth oxides are thermally stable compounds and rare earth metals readily form the oxides when in contact with oxygen. However, the oxides form hydroxides and carbonates with water vapor and carbon dioxide in the atmosphere. The tendency to form carbonates and hydroxides decreases when moving from left to right in the lanthanide series, lanthanum having the highest tendency.[39] The hygroscopicity has been attributed to the lower electronegativity of the early lanthanides compared to the heavier ones.[40] Changes in the surface morphology of an annealed La_2O_3 film after exposure to air are shown in Figure 6. Formation of $La(OH)_3$ increases the roughness and decreases the permittivity of the film making the $La(OH)_3$ formation very undesirable in microelectronic applications.[41,42] To

suppress the moisture absorption of La_2O_3, ternary oxides such as $LaAlO_3$,[43,44] $LaLuO_3$ [45,46] and $La_yZr_{1-y}O_x$[47] have been studied. Suppression of the hygroscopicity has also been achieved with PrAlO films as compared to the plain PrO_x films.[48]

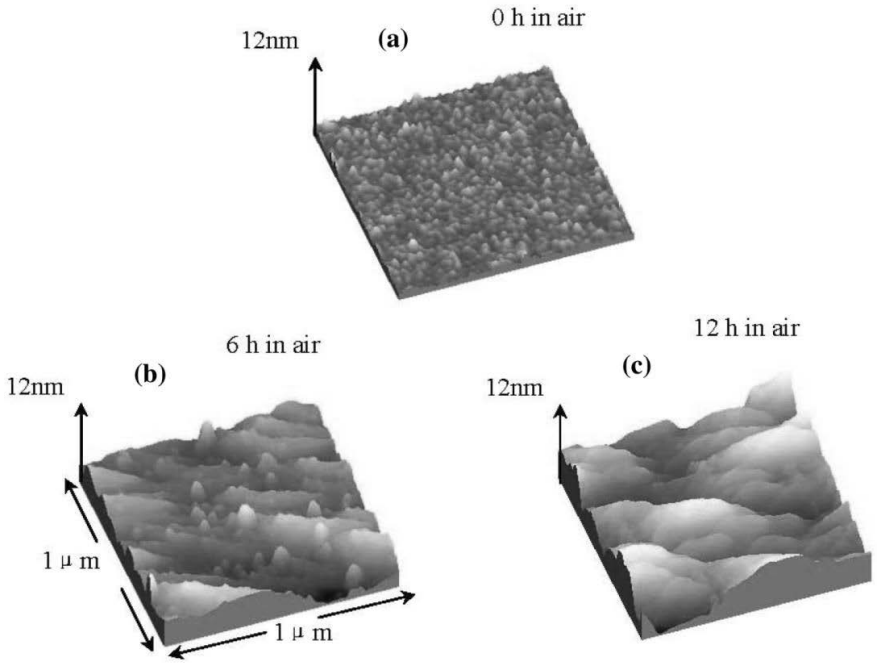

Figure 6. La_2O_3 film surface morphology after exposure to air for: a) 0 hours b) 6 hours and c) 12 hours. Reprinted from ref. 42 (MDPI publishing 2012).

3.2 Atomic layer deposition of rare earth oxides

Lanthanide 3+ ions are large and have high coordination numbers which favors the use of bidentate ligands to avoid oligomerization which leads to poorly volatile compounds. ALD of lanthanide oxides has been quite difficult because of the hygroscopicity of the films. This can lead to uncontrolled reactions: water is absorbed during the water pulse and if the purge period between the precursor pulses is not long enough, desorption continues during the next pulse allowing reaction between water and metal precursor destroying the self-limiting growth. [43] With ozone, carbonates have been observed to form along with oxides.[19] Also, Pr and Tb oxide films have been reported to have thickness gradients across the substrate when ozone is used as the oxygen source in cross-flow ALD reactors. The ability to adopt mixed oxidation state makes Pr and Tb oxides catalytically active, which may explain the nonuniformity of the films.[49]

$RE(thd)_x$ precursors are the most studied for RE oxides and almost all RE metals have an ALD precursor with thd ligands.[49,50,51] These precursors typically have high thermal stability, but unfortunately the growth rates are very low, in the range of 0.2 – 0.4 Å/cycle. Praseodymium and terbium oxides have been shown to crystallize to RE_6O_{11} and PrO_2 phases instead of the RE_2O_3 phase usually seen for the rare earth oxides.
There are not many examples of rare earth alkoxide precursors, $Lu(O^iPr)_3$ and $Gd(dmb)_3$ (dmb = 2,3-dimethyl-2-butokside) representing the few.[52,53] Many alkoxides of rare earths form oligomers that have low volatility and hence are not suitable as ALD precursors.[54] In the study on the $Lu(O^iPr)_3/H_2O$ process, no other details of the process were given except the deposition temperature (330 °C).[52] The $Gd(dmb)_3/H_2O$ process was studied at deposition temperatures of 250 – 400 °C and saturation of the growth rate was tested at 400 °C. The growth rates with different pulse lengths were scattered but no obvious trend of increasing growth rate with increasing $Gd(dmb)_3$ pulse length indicating thermal decomposition of the precursor was observed.[53]

A donor functionalized alkoxide precursor, $Ce(mmp)_4$ (mmp = 1-methoxy-2-methyl-2-propanolate) has been used in the ALD of CeO_2 together with water using liquid injection delivery.[55] In this method, the metal precursor is dissolved in a solvent which is then injected into the evaporator. Liquid injection can enable the use of less thermally stable and less volatile precursors.[56] ALD-type growth of CeO_2 was confirmed at 300 °C with a growth rate of 1.2 Å/cycle.[55] Other rare earth mmp precursors, namely $Pr(mmp)_3$ and $Gd(mmp)_3$ have also been studied in liquid injection ALD of PrO_x and Gd_2O_3 but saturation was not achieved.[56]

Cyclopentadiene precursors have gained a lot of interest in the recent years.[57] In general, they show much higher growth rates than the $RE(thd)_x$ precursors and can be used with water or ozone. However, their thermal stability is often lower than that of the thd precursors. In some cases, even though self-limiting growth has not been achieved, films with good uniformity and low impurity levels have been reported. For example, Niinistö et al. reported low carbon impurity content of 0.5 at% and thickness nonuniformity less than 2 % along the gas-flow direction for the $Gd(CpMe)_3/H_2O$ process even though self-limiting growth was not observed.[51]

From the precursors with M-N bonds, simple rare earth alkylamides, $RE(NR_2)_3$, are unstable and involatile.[58] However, silylamide precursors, $RE[N(SiMe_3)_2]_3$, have been studied for La, Pr and Gd with water as the oxygen source. Unfortunately, self-limiting growth was not observed, and the films contained some residual Si.[58,59,60]

Amidinates NR(CR´)NR and guanidinates NR(CNR´$_2$)NR have been studied successfully for the growth of various RE oxides. $RE(DPDMG)_3$ precursors (DPDMG=N,N′-diisopropyl-2-dimethylamido-guanidinate) have been studied for Y, Gd and Dy. [61,62,63] Self-limiting growth was reported at temperatures of 225 – 250 °C with growth rates of 1.0 – 1.1 Å/cycle depending on the metal. Acetamidinate compounds RE tris(N,N′-diisopropylacet-amidinato) ($RE(amd)_3$) have been reported for many rare earth metals. Self-limiting growth has been observed around 300 °C for Sc_2O_3 and Y_2O_3 films with water as the oxygen

source.[64,65] In contrast, praseodymium acetamidinate/H_2O process was not self-limiting because of the absorption of water by the film.[48] $La(amd)_3$ was used together with water to deposit La_2O_3/Al_2O_3 nanolaminates[43]. By depositing only thin layers of La_2O_3 and Al_2O_3 in between, the absorption of water was minimized and the water could be desorbed without excessively long purge times and self-limiting growth was achieved at 330 °C with a growth rate of 0.8 Å/cycle estimated for the La_2O_3 part.[43] ALD processes for RE oxides using homoleptic metal precursors are collected in Table 2.

Table 2. Thermal ALD processes reported for RE oxides using homoleptic RE precursors.

	Precursor	Oxygen source	Studied T range (°C)	Self-limiting growth confirmed (°C)	Growth rate (Å/cycle)[a]	Ref.
Sc	$Sc(thd)_3$	O_3	250 – 500	375	0.13	66
	$Sc(Cp)_3$	H_2O	175 – 500	300	0.75	66
	$Sc(^iPrCp)_3$	O_3	250 – 400	2 different precursor doses studied	0.7 (300)	67
	$Sc(MeCp)_3$	H_2O	250 – 350	300	0.65	57, 68
	$Sc(^iPramd)_3$	H_2O	290 – 360	290	0.3	64
Y	$Ythd_3$	O_3	200 – 425	350	0.23	69
	$Y(thd)_3(bipy)$	O_3	200 – 425	350	0.23	69
	$Y(thd)_3(phen)$	O_3	200 – 425	350	0.22	69
	YCp_3	H_2O	175 – 500	250, 300	1.5 – 1.6	70
	$Y(MeCp)_3$	H_2O	175 – 450	250, 300	1.3	70
	$Y(EtCp)_3$	H_2O	150 – 400	250	1.7	71
	$Y(^iPrCp)_3$	O_3	200 – 350	270	1.7	72
	$Y(^iPramd)_3$	H_2O	150 -330	280	0.8	65
	$Y(DPDMG)_3$	H_2O	150 – 280	225	1.1	61
La	$La(thd)_3$	O_3	180 – 425	250	0.36	19
		H_2O	230 – 350	270	0.35	73
	$La(Cp)_3$	H_2O	260	not studied	-	74
	$La(CpMe_4)_3$	H_2O	200	decomposing	-	80
	$La(^iPrCp)_3$	O_3	150 – 300	225	0.6	67
		H_2O	200 – 400	300	1.5	75
	$La[N(SiMe_3)_2]_3$	H_2O	150 – 250	not self-limiting	0.35 (225)	59
	$La(^iPrfamd)_3$	O_3	200 – 250	250	1.0	76
		H_2O	200 – 250	-	0.2	76
	$La(^iPramd)_3$*	H_2O	300 – 330	330	0.8	43
Ce	$Ce(thd)_4$	O_3	175 – 375	250	0.32	77
	$Ce(thd)_3phen$	O_3	225 – 350	275	0.42	77
	$Ce(mmp)_4$	H_2O	300	300	1.2	55
Pr	$Pr(thd)_3$	O_3	190 – 350	not self-limiting	0.52 (200)	78
	$Pr(EtCp)_3$	H_2O	130, 180, 250	130	0.7	79
	$Pr(^iPrCp)_3$	H_2O	175 – 225	not self-limiting	1.6 (175)	80
	$Pr(^iPramd)_3$	H_2O	200 – 315	not self-limiting	1.3 (?)	48
	$Pr[N(SiMe_3)_2]_3$	H_2O	200 – 400	not self-limiting	0.3 (300)	60
	$Pr(mmp)_4$	H_2O	150 – 350	not self-limiting	Not reported	56

Nd	$Nd(thd)_3$	O_3	200 – 450	310	0.45	[81]
Sm	$Sm(thd)_3$	O_3	200 – 400	not studied	0.4 (300)	[49]
Eu	$Eu(thd)_3$	O_3	200 – 400	not studied	0.3 (300)	[49]
Gd	$Gd(thd)_3$	O_3	225 – 400	300	0.3	[51]
	$Gd(CpMe)_3$	H_2O	150 – 350	not self-limiting	2.5 (250)	[51]
	$Gd(^iPrCp)_3$	O_3	250	not self-limiting	2.5 (250)	[82]
		H_2O	200 – 350	not self-limiting	1 (300)	[57]
	$Gd(dmb)_3$	H_2O	300 – 400	400	0.4	[53]
	$Gd(DPDMG)_3$	H_2O	150 – 300	225, 250	1.1	[62,63]
	$Gd[N(SiMe_3)_2]_3$	H_2O	150 – 300	not self-limiting	1.4 (200)	[58]
	$Gd(mmp)_3$	H_2O	200 – 300	not self-limiting	0.3 (225)	[56]
Tb	$Tb(thd)_3$	O_3	200 – 400	not self-limiting	0.85 (300)	[49]
Dy	$Dy(thd)_3$	O_3	200 – 400	not studied	0.3 (300)	[49]
	$Dy(DPDMG)_3$	H_2O	150 – 350	225, 250	1.0	[63]
Ho	$Ho(thd)_3$	O_3	200 – 400	not studied	0.3 (300)	[49]
Er	$Er(thd)_3$	O_3	200 – 450	not studied	0.25 (300)	[83]
	$Er(CpMe)_3$	O_3	100 – 400	not studied	1.2 (250)	[95]
		H_2O	175 – 450	250, 300	1.5	[94]
	$Er(Cp^iPr)_3$	O_3	200 – 300	250	0.4	[92]
		H_2O	200 – 300	250	1.0	[92]
	$Er(Cp^nBu)_3$	O_3	225 – 375	275	0.8	[92]
		H_2O	225 – 400	275	1.4	[92]
	$Er(^tBuamd)_3$	O_3	225 – 300	not self-limiting	~0.4 (250)	[84]
	$Er(DPDMG)_3$	H_2O	150 – 350	200, 225, 250	1.1	[85]
Tm	$Tm(thd)_3$	O_3	200 – 400	not studied	0.2 (300)	[49]
	$Tm(Cp)_3$	H_2O		200 – 300	1.5	[86]
Yb	$Yb(thd)_3$	O_3	200 – 400	300, 350	0.15	[87]
	$Yb(CpMe)_3$	H_2O	200 – 400	250	1.0	[67]
Lu	$Lu(thd)_3$	O_3	300	300	0.23	[88]
	$Lu(^iPrCp)_3$	O_3	200 – 330	250	0.75	[89]
		H_2O	not reported	not self-limiting	0.3 (250)	[89]

[a]Growth rate at self-limiting growth conditions. If no self-limiting growth is detected or studied, marked is the growth rate at the temperature which is shown in parenthesis (°C). * Growth rate estimated from $La_xAl_{2-x}O_3$ deposition

Table 3 summarizes the few heteroleptic precursors used in the ALD of RE oxides. Very recently, Rahman et al. studied heteroleptic scandium precursor $Sc(MeCp)_2(Me_2pz)$ (Me_2pz = 3,5-dimethylpyrazolate).[90,91] This precursor was designed to improve the reactivity of $Sc(MeCp)_3$. It was shown that saturative chemisorption is achieved on a SiO_2 surface after 1 s pulse above 150 °C and the resulting surface species are stable up to 400 °C.[91] ALD growth was studied with ozone but only 20 cycles were made. Self-limiting growth mechanism was reported but because the scandium precursor was shown to react directly with the SiO_2 native oxide on the surface of the silicon substrate forming $ScSi_yO_x$, and ozone oxidized the underlying Si substrate through the 20 cycle experiment, growth rate of the Sc_2O_3 film could not be derived.[90]

A heteroleptic erbium precursor, Er(MeCp)$_2$(^{i}Pr-amd) was studied by Blanquart et al.[92] Self-limiting growth was obtained at 250 °C with both water and ozone as the oxygen source. The growth rates were 0.4 Å/cycle with O_3 and 1.2 Å/cycle with H_2O. Oh et al. studied the same Er precursor with water as the oxygen source.[93] They reported constant growth rate of around 0.5 Å/cycle between 180 and 250 °C and a decrease in growth rate from 0.5 Å/cycle to 0.2 Å/cycle when the temperature was increased to 320 °C. Self-limiting growth was confirmed at 180 °C by Oh et al. Blanquart et al. reported a slight increase in the growth rate from 1.10 to 1.35 Å/cycle between 225 and 325 °C with water.[92] The growth rate is more than doubled compared to the work of Oh et al. No obvious reason for the different growth rates could be found from the articles. It could be partially related to the different ALD reactor types used in the two studies.

The homoleptic counterpart of the Er(MeCp)$_2$(^{i}Pr-amd) precursor, Er(MeCp)$_3$ has been studied previously with water or ozone as the oxygen source.[94,95] With water, self-limiting growth was confirmed with a growth rate of 1.5 Å/cycle at 300 °C.[94] The growth rate is slightly higher than that reported for the Er(MeCp)$_2$(^{i}Pr-amd)/H_2O process by Blanquart et al. With ozone, the growth rate was reported to be three times higher than with the heteroleptic precursor over a wide temperature range from 170 to 330 °C but unfortunately the growth rate saturation was not studied.[95] Er(^{i}Pr-amd)$_3$ has not been reported in ALD of Er_2O_3 but another amidinate, Er(^{t}Bu-amd)$_3$ [tris(*N*,*N*′-di-tert-butylacetamidinato)erbium] has been studied with ozone.[84] The growth rate was 0.39 Å/cycle at 250 °C but self-limiting growth could not be confirmed. Interestingly, the growth rate was around 0.4 – 0.5 Å/cycle depending on the precursor pulse length, which is in the same range as with the heteroleptic Er(MeCp)$_2$(^{i}Pr-amd)/O_3 process at the same temperature.[92]

Scarel et al. have studied heteroleptic Lu precursor, dimeric {Lu[Cp(SiMe$_3$)]$_2$Cl}$_2$.[96] Lu_2O_3 film deposition from {Lu[Cp(SiMe$_3$)]$_2$Cl}$_2$ with water as the oxygen source was reported only at a temperature of 360 °C and no evidence of self-limiting growth was shown.[96]

The heteroleptic Y precursor Y(^{i}PrCp)$_2$(^{i}Pr-amd) reported in Publication I in this thesis has been studied previously with water.[97,98] Park et al. reported ALD of Y_2O_3 at a temperature range 250 – 450 °C. The growth rate decreased with increasing deposition temperature and self-limiting growth with a rate of 0.6 Å/cycle was obtained at 350 °C.[97] The saturation temperature was the same as in I but otherwise these results were somewhat different compared to the Publication I in this thesis. In I, the growth rate was observed to increase with increasing temperature from 200 to 350 °C. Decrease in growth rate with increasing temperature was not observed with any of the studied RE(^{i}PrCp)$_2$(^{i}Pr-amd) precursors.[I,II,IV] Also, the growth rate in Publication I was twice as high as the one obtained by Park et al. Lee et al. studied the Y(^{i}PrCp)$_2$(^{i}Pr-amd)/H_2O process at 180 °C. They reported self-limiting growth with a rate of 0.4 Å/cycle.[98] In Publication I the lowest deposition temperature with water was 200 °C and the growth rate at this temperature was 0.7 Å/cycle.

Dy(^{i}PrCp)$_2$(^{i}Pr-amd), which in Publication I is shown to give growth rates between 0.8 and 1.4 Å/cycle when used with water at 200 – 350 °C, was previously reported to result in growth rates around 0.3 Å/cycle in plasma enhanced ALD at a deposition temperature range

of 150 – 230 °C, but no growth with water was achieved.[93] Unfortunately, the deposition conditions and temperatures that were tried with the Dy(^{i}PrCp)$_2$(^{i}Pr-amd)/H_2O process were not mentioned in the article so a comparison between Ref. 93 and I is not possible. More detailed results of the Y, Dy and other heteroleptic RE precursors studied in this thesis (publications I, II, IV) are discussed in Chapter 7.

Table 3. Heteroleptic RE precursors studied for thermal ALD of binary rare earth oxides.

	Precursor	Oxygen source	Studied T range (°C)	Self-limiting growth confirmed (°C)	Growth rate (Å/cycle)[a]	Ref.
Sc	Sc(MeCp)$_2$(Me$_2$pz)	O_3	225, 275	275	-	90
Y	Y(^{i}PrCp)$_2$(^{i}Pr-amd)	H_2O	250 – 450	350	0.6	97
	Y(^{i}PrCp)$_2$(^{i}Pr-amd)	O_3	220 – 350	350	1.3	I
		H_2O	200 – 350	350	1.2	I
La	La(^{i}PrCp)$_2$(^{i}Pr-amd)	O_3	200 – 325	225	1.0	II
		H_2O	200 – 300	not self-limiting	1.25 (200)	
		H_2O/O_3	200 – 325	200	0.7	
		EtOH	200 – 300	not self-limiting	1.3 (275)	
Pr	Pr(^{i}PrCp)$_2$(^{i}Pr-amd)	O_3	200 – 250	not self-limiting	-	I
		H_2O	200 – 300	not self-limiting	~1 (200)	
Gd	Gd(^{i}PrCp)$_2$(^{i}Pr-amd)	O_3	200 – 350	225	0.8	I
		H_2O	200 – 325	not self-limiting	~0.7 (200)	
Dy	Dy(^{i}PrCp)$_2$(^{i}Pr-amd)	H_2O	Not reported		No growth	93
	Dy(^{i}PrCp)$_2$(^{i}Pr-amd)	O_3	200 – 350	not self-limiting	1 (300)	I
		H_2O	200 – 350	not self-limiting	1.3 (300)	I
Er	Er(MeCp)$_2$(^{i}Pr-amd)	O_3	200 – 325	250	0.4	92
		H_2O	225 – 325	250	1.4	92
	Er(MeCp)$_2$(^{i}Pr-amd)	H_2O	130 – 320	180	0.5	93
Lu	{Lu[Cp(SiMe$_3$)]$_2$Cl}$_2$	H_2O	360	not studied	0.25 (360)	96

[a]Growth rate at self-limiting growth conditions. If no self-limiting growth is detected or studied, marked is the growth rate at the temperature which is shown in parenthesis (°C). - film thickness could not be measured due to too thin samples (Sc) or nonuniformity (Pr).

4 Zirconium dioxide thin films

4.1 Properties of zirconium dioxide

Zirconium is the element number 40 and in the periodic table it is next to yttrium (Figure 5). Zirconium has one stable oxidation state, +4.[99] Zirconium oxide has three different crystalline phases in normal pressure; monoclinic, tetragonal and cubic, and a fourth phase in high pressure, orthorhombic ZrO_2. In bulk ZrO_2, the monoclinic phase is stable at room temperature and the tetragonal and cubic phases at high temperatures. Phase changes in ZrO_2 generate high volume changes inducing cracks. For many applications the phase of zirconia needs to be stabilized. Often a small amounts of tri- or divalent cations are added to ZrO_2 as dopants to stabilize the phase and to prevent the phase changes. When Zr^{4+} ions in the crystalline lattice are replaced by lower valence ions, oxygen vacancies are formed which leads to the phase stabilization.[100]

In thin films, factors that may affect the phase stability include stress, grain size, impurities, deposition process in general, substrate and thickness.[101] In very thin films and nanoparticles the surface area to bulk ratio becomes high which favors crystalline phases with lower surface energy. Figure 7 shows particle sizes and film thicknesses at which monoclinic, tetragonal and amorphous zirconia are the most stable phases. For the tetragonal ZrO_2 films the range is approximately between 3 and 15 nm, whereas in thicker films the monoclinic phase is the most stable.[99] However, the other factors that affect the phase formation also need to be considered and for that reason, studies of deposition process conditions and precursor combinations are pivotal.

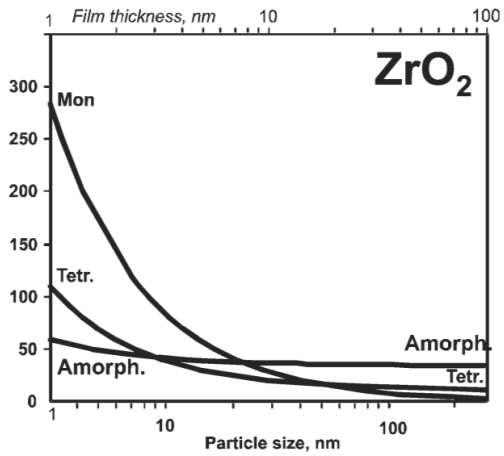

Figure 7. Enthalpy of nanophase zirconia plotted *versus* particle size (film thickness). Reproduced from Ref. 99 with permission from The Royal Society of Chemistry.

ZrO_2 has high relative permittivity, high thermal stability and a large band gap of 5.8 eV.[102] These properties make it a good dielectric material for microelectronic applications. The permittivity is dependent on the crystalline phase. The high permittivity phases are desirable in microelectronics. The tetragonal zirconia has the highest permittivity of the three phases, above 40, the cubic phase above 30, and the monoclinic phase around 20 in bulk form. In thin films there are many factors affecting the permittivity and for example for the cubic and tetragonal phases values between 20 and 40 have been measured.[101,103,104]

4.2 Atomic layer deposition of zirconium dioxide

Zirconium dioxide is very interesting material for microelectronics, which is probably the root cause why Zr precursors have been synthesized and studied so extensively. The first ALD Zr precursor was $ZrCl_4$.[105] $ZrCl_4$ has been studied in a wide temperature range from 180 to 600 °C.[17,18] Self-limiting growth has been confirmed as high as at 500 °C, demonstrating the excellent thermal stability of zirconium chloride. The produced ZrO_2 films have been reported to be of high purity with only small amounts of chlorine as an impurity.[105] However, the HCl byproduct is corrosive and small precursor particles have been shown to transfer sometimes from the source to the substrate and incorporate in the film.[3] From the halide family, also ZrI_4 has been studied as a zirconium source for ALD. The first studies were conducted with H_2O-H_2O_2 solution as the oxygen source. Growth rates around 0.8 Å/cycle were reported above 300 °C. Iodine impurities (0.8 – 1.3 at%) were detected at deposition temperatures of 250 – 350 °C but not at 375 – 500 °C.[106] At a low deposition temperature of 275 °C the crystalline phase of the films was tetragonal ZrO_2 but at higher temperatures also monoclinic phase was seen.[107]

$Zr(thd)_4$ has quite high thermal stability (375 °C) and the films produced with the $Zr(thd)_4/O_3$ process have low impurity contents of less than 0.5 at% of carbon and hydrogen.[108] However, the growth rate is low, 0.24 Å/cycle, similar to the rare earth oxide films deposited with $RE(thd)_3/O_3$ processes. Zirconium amidinate precursor, namely tetrakis(*N*,*N*′-dimethylacetamidinate) zirconium, shows self-limiting growth with H_2O at 300 °C, but also with a low growth rate of 0.24 Å/cycle.[109]

From the alkoxide family, zirconium tert-butoxide $Zr(O^tBu)_4$ has been studied as an ALD precursor for the ZrO_2 deposition. High dielectric constant of 32 was obtained with the $Zr(O^tBu)_4/H_2O$ process but self-limiting growth was not achieved in the deposition range of 150 – 300 °C. The growth rate was highly dependent on the deposition temperature and above 300 °C the growth rate was zero due to $Zr(O^tBu)_4$ decomposition before reaching the substrate.[110]

Hausmann et al. reported the synthesis of three alkylamide precursors, $Zr(NMe_2)_4$, $Zr(NEtMe)_4$ and $Zr(NEt_2)_4$, and their use in atomic layer deposition of ZrO_2 with water.[111] Especially the $Zr(NEtMe)_4$ precursor (TEMAZ) has been widely used in the studies of ZrO_2 films for microelectronic applications.[112,113] Films with good purity and a growth rate of

1 Å/cycle have been produced but the thermal stability of TEMAZ is limited to below 300°C.[114,115] Table 4 lists some examples of the different types of homoleptic precursors used for the ALD of ZrO_2.

Table 4. Examples of thermal ALD processes for ZrO_2 using homoleptic Zr precursors from different ligand families.

Precursor	Oxygen source	Studied T range (°C)	Self-limiting growth confirmed (°C)	Growth rate (Å/cycle)[a]	Ref.
$ZrCl_4$	H_2O	500, 180 - 600	500	0.53	105,**Virhe. Kirjanmerkkiä ei ole määritetty.**
$Zr(thd)_4$	O_3	275 – 500	375	0.24	108
$Zr(NEtMe)_4$	O_3 H_2O	300 150 – 350	Not self-limiting Not studied	1.1 (265) 1 (250)	115 111
$Zr(Me_2amd)_4$	H_2O	150 – 350	300	0.24	109
$Zr(O^tBu)_4$	H_2O	150 – 325	Not self-limiting	0.75 (250)	110

Unlike in the case of the rare earths, heteroleptic zirconium precursors have been widely studied (Table 5). In general, low impurity levels are often reported for zirconia processes. ZrO_2 is not hygroscopic in the way as many lanthanide oxides are and it does not react with CO_2 in air either to form carbonates.

While the zirconium ion is too small for homoleptic zirconium precursors with four Cp ligands to exist, majority of the heteroleptic zirconium precursors have Cp rings as one of the ligands. The studied precursors include combinations of Cp-alkyl, Cp-halogen, Cp-alkylamide, Cp-cycloheptatrienyl (CHT) and three ligand combinations Cp-alkyl-alkoxide. Cp-alkylamide precursors with three NMe_2 ligands and one CpR ligand (R=H, methyl or ethyl) have been reported to deposit ZrO_2 films with low impurity levels, high-κ cubic crystalline phase and a growth rate of 0.9 Å/cycle at 300 °C.[114] Higher saturation temperature but lower growth rate of around 0.5 Å/cycle has been demonstrated with Cp-alkyl precursors. $ZrCp_2Me_2$ and $Zr(CpMe)_2Me_2$ both showed self-limiting growth at 350 °C with water [116,117] or ozone[108,118] as the oxygen source. Self-limiting growth at 350 °C was also reported with the $Zr(CpMe)CHT/O_3$ process with a growth rate of 0.8 Å/cycle.[119] It seems that 350 °C is the limit for the self-limiting growth for the current heteroleptic zirconium precursors.

Four precursors with three different ligands have been studied: $Zr(CpMe)_2(OMe)Me$ with water or ozone, $ZrCp_2(OMe)Me$ with ozone, $Zr(CpMe)_2(O^tBu)Me$ with water, and $Zr(Cp_2CMe)_2(OMe)Me$ with ozone as the oxygen source. Only $Zr(CpMe)_2(OMe)Me$ showed self-limiting growth with rates of 0.50 and 0.65 Å/cycle with water and ozone at 350 °C.[117,118] The saturation temperature is the same as for the two ligand analog

$Zr(CpMe)_2Me_2$ but $Zr(CpMe)_2(OMe)Me$ has slightly higher growth rate with ozone. The $ZrCp_2(OMe)Me/O_3$ process was studied at 300 °C.[47] The main focus of the article was on ternary $La_yZr_{1-y}O_x$ and no details on the ZrO_2 deposition were given. However, the ZrO_2 films were crystalline with a tetragonal phase and a dielectric constant of 30.[47] $Zr(Cp_2CMe)_2(OMe)Me$ is an ansa-metallocene precursor with bridged Cp ligands. It has been studied in the liquid injection ALD with ozone as the oxygen source.[120] The deposited films were oxygen deficient with an O:Zr ratio of 1.62 while the stoichiometric value is 2.0. $Zr(Cp_2CMe)_2Me_2$ was examined in the same study and was also found to result in low O:Zr ratio of 1.57. Saturation of the growth rate was not studied. In contrast, liquid injection ALD using the $Zr(CpMe)_2(O^tBu)Me/H_2O$ process produced films with excess oxygen, the O:Zr ratio being 2.55 at 300 °C and 3.54 at 350 °C.[121]

Of the few heteroleptic precursors without Cp ligands, the alkoxide-donor functionalized alkoxide precursors $Zr(^iPrO)_2(dmae)_2$ and $Zr(^tBuO)_2(dmae)_2$ did not show self-limiting growth when used with water as the oxygen source because of the low thermal stability of the alkoxide ligands.[122,123] Similar problem was seen with the homoleptic alkoxide precursor $Zr(O^tBu)_4$.[110] Zirconium precursor with chloride and silylamide ligands $Zr[N(SiMe_3)_2]_2Cl_2$ did show saturation with H_2O at 250 °C with a high growth rate of 1.1 Å/cycle. However, 4 at-% of Si impurities were detected in the films at this temperature.[124]

Quite recently, two heteroleptic amido-guanidinate precursors have been studied, namely $Zr(NEtMe)_2(guan\text{-}NEtMe)_2$ and $Zr(NEtMe)_3(guan\text{-}NEtMe)$.[125,126] Both precursors showed self-limiting growth with water or ozone as the oxygen source and had higher growth rates with ozone than with water. The growth rates were 0.8 – 0.9 Å/cycle with water and 1.0 – 1.15 Å/cycle with ozone at the deposition temperaturse of the self-limiting growth. $Zr(EtMeN)_2(guan\text{-}NEtMe)_2$ was thermally slightly more stable as saturation was achieved at 300 °C compared to 275 °C with $Zr(NEtMe)_3(guan\text{-}NEtMe)$. Film purity was better with ozone compared to water with both precursors. A similar trend in the impurity levels was also observed in publication II in this thesis work.

Table 5. Heteroleptic Zr precursors studied for thermal ALD of ZrO_2.

Precursor	Oxygen source	Studied T range	Self-limiting growth confirmed (°C)	Growth rate (Å/cycle)[a]	Ref.
$Zr(^iPrO)_2(dmae)_2$	H_2O	190 – 340	not self-limiting	1.0 (240)	122
$Zr(^tBuO)_2(dmae)_2$	H_2O	190 – 340	not self-limiting	0.9 (240)	122,123
$ZrCp_2Me_2$	H_2O	200 – 500	350	0.43	116
	O_3	250 – 500	350	0.55	108
$Zr(CpMe)_2Me_2$	H_2O	300 – 500	350	0.50	117
	O_3	250 – 500	350	0.55	118
$Zr(Cp_2CMe)_2Me_2$	O_3	175 – 350	not reported	not reported	120
$ZrCp_2Cl_2$	O_3	200 – 500	300	0.53	108
$ZrCp(NMe_2)_3$	O_3	250 – 400	300	0.9	114
$Zr(CpMe)(NMe_2)_3$	O_3	250 – 400	300	0.9	114
$Zr(CpEt)(NMe_2)_3$	O_3	250 – 400	300	0.9	114
Zr(CpMe)CHT	O_3	250 – 475	350	0.8	119
$Zr(Me_5Cp)(TEA)$	H_2O	400 – 425	not self-limiting	0.1 (400)	III
	O_3	250 – 425	300 – 375	0.3 – 0.4	
Zr(MeCp)(TMEA)	H_2O	200 – 375	not self-limiting	0.5 (300)	
	O_3	200 – 375	not self-limiting	0.25(300)	
$Zr(EtMeN)_2(guan\text{-}NEtMe)_2$	H_2O	250 – 400	300	0.9	125
	O_3	250 – 400	300	1.15	
$Zr(EtMeN)_3(guan\text{-}NEtMe)$	H_2O	225 – 350	275	0.8	126
	O_3	225 – 350	275	1.0	
$Zr\ [N(SiMe_3)_2]_2Cl_2$	H_2O	150 – 350	250	1.1	124
$Zr(CpMe)_2(OMe)Me$	H_2O	300 – 500	350	0.5	117
	O_3	250 – 500	350	0.65	118
$ZrCp_2(OMe)Me$	O_3	300	not reported	not reported	47
$Zr(CpMe)_2(O^tBu)Me$	H_2O	250 – 450	not studied	not reported	121
$Zr(Cp_2CMe)_2\ (OMe)Me$	O_3	200 – 350		not reported	120
$Zr(Cp)(^tBuDAD)(O^iPr)$	H_2O	250 – 425	not self-limiting	0.43 (300)	III
	O_3	250 – 375	250	0.5	III

[a]Growth rate at self-limiting growth conditions. If no self-limiting growth is detected or studied, shown is the growth rate at the temperature which is marked in parenthesis (°C).

5 Applications of rare earth and zirconium oxide thin films

Rare earth oxides and ZrO_2 are very versatile materials with applications in various fields. Examples are luminescent materials, catalysts, protective layers and constituents in solid oxide fuel cells and oxide superconductors.[127] More than a decade, they have been studied extensively as dielectric materials for microelectronics in both silicon and high mobility semiconductor-based devices.[13] In this chapter, the use of rare earth and zirconium oxide films in microelectronics and solid oxide fuel cells is discussed in more detail.

5.1 Microelectronics

5.1.1 MOSFET

The fast evolution of smart phones and computers in general is due to the development of semiconductor industry which has been guided by Moore´s law.[128] In 1965 Gordon Moore predicted that the number of metal-oxide-semiconductor field-effect transistors (MOSFET) in an integrated circuit doubles every year. Later he changed the prediction so that the doubling happens every two years. This has been the target of the industry ever since. To fulfill this expectation, sizes of the transistors have needed to shrink. Shrinking the devices increases the speed of the circuit and memory capacity and reduces the cost per bit. Silicon has been the choice of the semiconductor material for decades with silicon oxide SiO_2 as the dielectric gate oxide. However, the limits of this pair have been reached. The SiO_2 gate oxide has become so thin that direct tunneling of electrons and holes through the gate oxide cannot be avoided causing unbearable increase in leakage current.[129]

By using a high-κ material, the dielectric layer can be thicker with similar capacitance as achieved with a thinner SiO_2 layer. This can be exemplified with a parallel plate capacitor. The capacitance C of the capacitor depends on the distance d between the plates i.e. the thickness of the dielectric, the relative permittivity ε_r of the dielectric and the area A of the plates:

$$C=\varepsilon_0\varepsilon_r\frac{A}{d}, \qquad (1)$$

where ε_0 is the permittivity of the vacuum. From equation (1) it is seen that a capacitor with a high-κ dielectric reaches the same capacitance as a capacitor with SiO_2 dielectric with a thicker high-κ film. In a transistor one of the metal plates is replaced by a semiconductor.
Simply put, MOSFETs consist of a source, drain, channel, gate and gate dielectric (Figure 8). Source and drain are p- or n-type areas on a semiconductor substrate that has been doped with the opposite type of carriers. The SiO_2 or high-κ dielectric layer (gate oxide) lies between the substrate and the gate. With a certain gate voltage, electric field affecting through the gate oxide creates an inversion layer of the minority charge carriers on the interface of the gate oxide and substrate that serves as a channel for the carriers to move from the source to drain. Transistor acts as a digital switch that is turned on and off by changing the gate voltage.[130] High-κ gate oxide was taken into high volume manufacturing for the first time in 2007.[131]

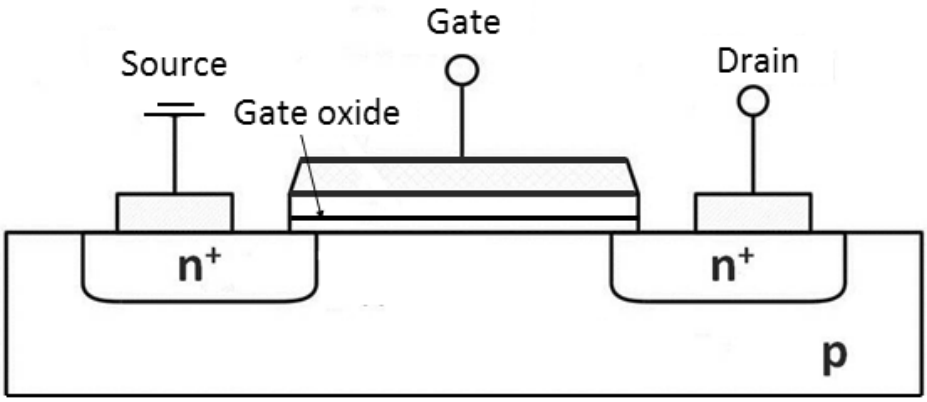

Figure 8. A schematic of a MOSFET structure.

The first high-κ oxides were hafnium based oxide materials. For the second generation, rare earth oxides and ternary or doped oxides have been considered. From the rare earth oxide family, La_2O_3 has been especially interesting since it is stable in the hexagonal crystal structure having considerably higher permittivity than the cubic phase where most of the rare earth oxides crystallize.[13] Unfortunately, rare earth oxides have been observed to form silicates during post deposition annealing.[132] The tendency to form silicates increases with increasing ion radius. Lanthanum has the largest radius of the rare earth oxides and hence the highest affinity towards Si atoms. Lamanga et al. reported high permittivity of 24 and 22 for ALD La_2O_3 thin films in metal-oxide-semiconductor capacitors on Si and Ge, but reactions with the substrate were observed in both cases: silicates and germanates were spontaneously formed during the film growth and annealing after the deposition.[133] While silicates decrease the overall permittivity of the dielectric stack compared to La_2O_3 films without interfacial layer, they can improve the device performance by preventing electron mobility reduction in the channel.[134]

To improve the stability as well as the dielectric properties, ternary rare earth containing oxides have been widely studied for microelectronics. $LaAlO_3$ has been successfully deposited to mitigate the hygroscopicity of La_2O_3.[43,44] $LaLuO_3$ films deposited by ALD on Si and GaAs substrates have shown high dielectric constants of around 30.[46,135] Rare earth scandates such as $GdScO_3$ and $DyScO_3$ have also been studied extensively. Higher dielectric constants than for the binary constituent oxides have been reported with values above 20 for RE scandate films deposited by ALD.[45,136] The scandates doped with large rare earth ions have shown higher crystallization temperature but also slightly higher carbon content than the scandates doped with small rare earth cations.[136] Amorphous films can reach lower leakage currents compared to crystalline films because of the lack of grain boundaries that act as leakage pathways. $GdScO_3$ and $YScO_3$ films deposited from the β-diketonate compounds $RE(thd)_3$ and ozone were reported to crystallize when annealed at 1000 °C.[137,138] Interestingly, when cyclopentadienyl precursors were used with water instead of $RE(thd)_3$ and ozone, crystallization of $YScO_3$ films was observed already at 800 °C. Films with low

carbon (<0.2 at%) and hydrogen (<1 at%) contents were deposited with both processes but the films deposited with the thd-based process had around 1 at% of fluorine as an additional impurity.[138]

RE oxides have also been utilized as dopants in HfO_2. For example, cerium and erbium doping of HfO_2 have been reported to stabilize the higher permittivity phases of HfO_2. Cerium doping stabilized the films in either the cubic or tetragonal phase depending on the cerium concentration with increased dielectric constant (39 at the highest) after annealing at 900 °C.[55] Erbium doped hafnia films were cubic with a dielectric constant of 27 before annealing and 33 after the annealing at 900 °C. Undoped HfO_2 films were deposited for comparison. They were monoclinic with dielectric constants of 18 and 16 before and after the annealing.[139]

While ZrO_2 is predominantly studied as a dielectric layer for memory applications, it has also been considered as a potential dielectric material for MOSFETs. ZrO_2 and HfO_2 are very similar to each other and form mixed oxides with any desirable metal ratio. Addition of zirconium to hafnium oxide has been reported to increase the film permittivity via stabilization of the tetragonal phase and to lower the threshold voltage shift as well as to increase the band gap.[140,141]

5.1.2 Memory devices

Dynamic random access memory (DRAM) has been the main memory of computers for decades. DRAM memory cell consists of a capacitor that is connected to a bit line via an access transistor connected to a word line and acting as a switch. The capacitor stores each bit of data as positive or negative electrical charge that is written and read through the bit line.[142] For a successful DRAM cell, two requirements need to be fulfilled: sufficient capacitance of 10 fF/cell and low leakage current of $< 10^{-7}$ A/cm^2 at the operating voltage.[142] ZrO_2 based materials, such as rare earth doped ZrO_2 and different stacked dielectric layers have been studied as the capacitor oxides in DRAMs.[143] The three layer ZrO_2–Al_2O_3–ZrO_2 (ZAZ) was shown to be an excellent dielectric for MIM capacitors and it replaced HfO_2 in the capacitors for the ≤45-nm technologynodes.[142,144,145] However, ZAZ is reaching the limit of scaling down and materials with higher κ, such as perovskites (κ values above 50) are needed in the future.[146]

Of the emerging non-volatile memory devices, zirconium oxide is a potential material for resistive switching random access memories (ReRAM). ReRAM cell consists of two electrodes and a thin film insulator between them. By applying a voltage across the electrodes, the electrical conductivity of the thin film material can be reversibly changed, and the corresponding conductance values can be stored for a long time.[147] In the metal-oxide-based ReRAM, a formation of a conductive filament is causing the conductivity in the originally insulating oxide layer.[148]

5.2 Solid oxide fuel cells

Both rare earth oxides and zirconia have been studied and used in solid oxide fuel cells (SOFC). SOFCs are electrochemical devices that transform chemical energy of fuel and oxidizer into electricity and heat. They can operate with several different fuels, for example H_2, CH_4 and CO. Molecular oxygen from air is used as the oxidizer.[149] As the name implies, SOFCs are all solid state, which makes them more robust in use than fuel cells and batteries with liquid electrolytes. SOFCs can be used in small scale portable charging systems, residential size power generator as well as in large scale power plants. They can also be used in combined heat and power plants.[150]

SOFCs consist of a cathode, an anode and an electrolyte between them (Figure 9). The electrodes are porous so that the gases can reach the electrolyte interface, but the electrolyte must be dense to avoid the mixing of the fuel and oxidizer. The electrolyte is an oxygen ion conductor that should not conduct electrons whereas the electrodes are electron conductors or mixed electron and oxygen ion conductors. The operation principle of SOFC is the following: O_2 is reduced at the cathode to O^{2-} ions which move through the electrolyte to the anode. At the anode the ions react with the fuel releasing electrons. Electrons are led through an external load to the cathode where they reduce oxygen.[151]

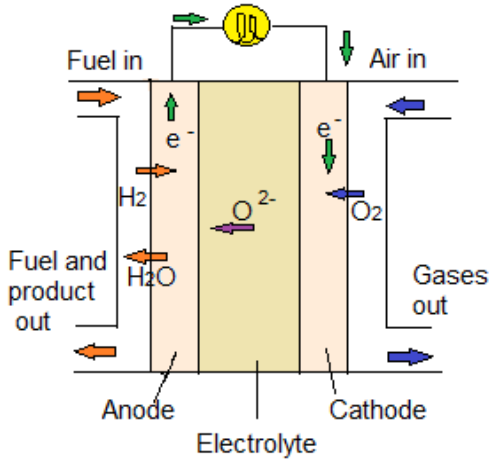

Figure 9. Operation principles of a solid oxide fuel cells using H_2 as the fuel.

Oxide compounds containing zirconium and rare earth elements have been studied especially as electrolyte materials for SOFCs. In high temperature SOFCs (700 – 1000 °C), yttria stabilized zirconia (YSZ) is the most used electrolyte material. It is chemically and thermally very stable and pure ion conductor in different oxygen partial pressures.[152] If the operating temperature is decreased, the ion conductivity decreases. However, lowering of the temperature increases the fuel cell lifetime and enables the use of less expensive materials as interconnects between the cells. YSZ can be used at lower temperatures if the electrolyte thickness is decreased to minimize the ohmic polarization at the electrolyte and

this way retain the power density.[153] Also other RE doped zirconia-based electrolytes have been studied for intermediate temperatures. Scandia stabilized zirconia has the highest oxide ion conductivity of all the stabilized zirconia materials. This is attributed to the low association enthalpy of defects because of the similar radii of Zr^{4+} and Sc^{3+} ions. The ionic conductivity of the ZrO_2-RE_2O_3 systems has been shown to decrease with increasing RE radius.[154]

For intermediate temperature SOFCs, doped cerium oxide has been widely studied. The most common dopant materials are Gd_2O_3, Sm_2O_3 and Y_2O_3. They all have high conductivity and are compatible with high performance electrode materials. However, under reducing conditions these materials become electron conductors which decreases the output voltage of the cell.[151] To overcome this problem, ceria electrolytes can be used together with thin YSZ electron blocking layers.[155,156]

Other RE containing materials for SOFC electrolytes are La containing perovskites such as $(La,Sr)(Ga,Mg)O_{3-x}$ and $La_2Mo_2O_9$. Both have been shown to have good ion conductivity but there are some concerns on the long term stability of these materials.[151]

In the traditional SOFCs, the electrolyte layer thickness varies from micrometers to a few hundreds of micrometers.[157] Layers with these thicknesses are not possible to deposit with ALD. However, thin film SOFCs, so called μ-SOFCs for portable use have been developed and can be fabricated using ALD.[158] The electrolytes need to be dense and producing dense films is one of the advantages of ALD. In a study by Park et al., thin film electrolytes deposited by ALD showed peak power densities over two times higher than electrolytes deposited by sputtering.[159] In addition to thin electrolytes, ALD deposited layers can also be used as diffusion and electron barriers between the electrodes and the electrolyte, protective layers for the interconnects and electrodes, and bonding layers and catalysts on the anode side enhancing the charge transfer in the oxidation of fuels.[155] In addition, the long term stability of some electrode materials has been enhanced with a thin and conformal ALD ZrO_2 coating.[160,161]

6 Experimental section

6.1 Precursors

All precursors as well as the thermogravimetric data and vapor pressures of the precursors were provided by Air Liquide. The data was collected with a Mettler Toledo TGA/DSC 1 STARe System. Measurements were done under nitrogen atmosphere with a nitrogen flow of 220 sccm/min in atmospheric pressure. TG analysis of $Zr(Me_5Cp)(TEA)$ was also done under vacuum at a pressure of 27 mbar. A heating program of 10 °C/min was used in all the measurements. Vapor pressures were estimated by using evaporation rate at each temperature.

6.2 Film depositions

All the films were deposited in a hot-wall cross-flow F-120 ALD-reactor (ASM Microchemistry, Ltd). Studied metal precursors were rare earth bisisopropylcyclopentadienyl-diisopropylacetamidinate, $RE(^iPrCp)_2(^iPr\text{-amd})$ (RE = Y, La, Pr, Gd or Dy), cyclopentadienyl N,N-bis(tertbutyl)ethene-1,2-diaminato isopropylalkoxo zirconium $Zr(Cp)(^tBuDAD)(O^iPr)$, methylcyclopentadienyl tris[2-(methylamino)ethyl]aminate zirconium Zr(MeCp)(TMEA) and pentamethylcyclo-pentadienyl triethoanolaminate zirconium $Zr(Me_5Cp)(TEA)$. The precursors and deposition parameters are listed in Table 6. The precursors were stored in a glove box under N_2 atmosphere. Water and ozone were tested as the oxygen source for all the oxides. Due to the hygroscopicity and easy carbonate formation of La_2O_3 films, their deposition was studied also with alternative oxygen sources, i.e. ethanol as well as water and ozone in the same process separated from each other with a purge period (later marked as H_2O/O_3). The pressure in the chamber was on the order of 5 mbar. Nitrogen (AGA, 99.999%; H_2O, ≤3 ppm; O_2, ≤3 ppm) was used as the carrier and purging gas. Ozone with a concentration of 100 g/m^3 was generated from O_2 (AGA, 99.999%) in an ozone generator (Wedeco Modular 4 HC). Soda lime glasses and Si(100) wafers cut to 5×5 cm^2 pieces were used as substrates. Native silicon oxide was not removed from the Si substrates before the depositions. For electrical measurements, ZrO_2 films were also deposited on Pt substrates.

Table 6. Rare earth oxide and Zr oxide processes studied in this thesis.

Precursor	Oxygen sources	Subl./Evap. temperature (°C)	Deposition temperatures	Publication
$Y(^iPrCp)_2(^iPr\text{-amd})$	O_3, H_2O	135	200 – 350	**I, IV**
$La(^iPrCp)_2(^iPr\text{-amd})$	O_3, H_2O, EtOH, H_2O/O_3	126	200 – 325	**II**
$Pr(^iPrCp)_2(^iPr\text{-amd})$	O_3, H_2O	125	200 – 300	**I, IV**
$Gd(^iPrCp)_2(^iPr\text{-amd})$	O_3, H_2O	117	200 – 350	**I, IV**
$Dy(^iPrCp)_2(^iPr\text{-amd})$	O_3, H_2O	135	200 – 350	**I**
$Zr(Cp)(^tBuDAD)(O^iPr)$	O_3, H_2O	65	250 – 425	**III**
Zr(MeCp)(TMEA)	O_3, H_2O	120	200 – 400	**III**
$Zr(Me_5Cp)(TEA)$	O_3, H_2O	115	250 – 425	**III**

6.3 Characterization of the films

Films were characterized for thickness, crystallinity, morphology, and composition. The analysis methods used in this work are summarized in Table 7. RE oxide film thicknesses were determined by modeling the reflectance spectra measured within wavelengths of 370 – 1100 nm with a spectrophotometer (Hitachi, Model U-2000). Some thicknesses were confirmed with X-ray reflectivity (XRR) measurement (PANalytical X´Pert Pro MPD). ZrO_2 film thicknesses were measured with XRR (Rigaku SmartLab). The crystallinity and phase of the films were determined by grazing-incidence X-ray diffraction (GIXRD) with a PANalytical X'Pert Pro MPD X-ray diffractometer with Cu Kα (λ = 1.5419 Å) radiation and incident beam angle of 1°. PANalytical Highscore Plus was used for phase identification using ICDD and ICSD databases. In situ high temperature XRD (HTXRD) measurements were conducted on La_2O_3 films with an Anton-Paar HTK1200N oven.

Morphologies of the Y_2O_3, ZrO_2, PrO_x, Gd_2O_3 and Dy_2O_3 films were studied by field-emission scanning electron microscope (Hitachi S-4800). 2 nm thick metal coating (Cressington 208HR sputter coater with a Au/Pd target) was sputtered on some samples to avoid charging and thereby improving the image quality. La_2O_3 film morphologies were studied with a Multimode V atomic force microscope (AFM) equipped with a NanoScope V controller (Veeco Instruments) operated in the tapping mode. Images (500×500 nm^2 and 2×2 μm^2) were captured in air using silicon probes with a nominal tip radius of 8 nm and a nominal spring constant of 3 N/m (VLFM or FESP from Bruker). Roughness was calculated as a root-mean-square value (RMS) from 2×2 μm^2 images (512×512 pixels) obtained at 0.5–1.0 Hz scan rate. Roughness calculations and image processing were done with a Bruker Nanoscope Analysis 1.5 program.

Film compositions were measured with time-of-flight elastic recoil detection analysis (TOF-ERDA) at a detection angle of 40° by 40 MeV $^{79}Br^{7+}$ ions obtained from a 5 MV tandem accelerator (Model EGP-10-II).

Annealing experiments were done on La_2O_3 films at 700 °C in air or in N_2 atmosphere for 1 h. After the annealing the films were let to cool down slowly in the oven. XRD and TOF-ERDA were measured also from the annealed samples.

Metal-insulator-metal (MIM) parallel plate capacitors with Pt/ZrO_2/Al structures were made for electrical measurements. ZrO_2 films were deposited on Pt (40 nm) that was evaporated on Si wafer and aluminum dots (90 nm thick) with an area of 0.204 mm^2 were e-beam evaporated through a shadow mask on top of the ZrO_2 films. Samples were handled in normal room air between the film deposition steps. Current-voltage (I – V) characteristics were measured with a Keithley 2400 source meter with a step size of 0.2 V. Capacitance values were measured with an HP4284A LCR meter with a frequency of 10 kHz. Relative permittivities were calculated from the mean capacitances.

Table 7. Characterization methods used in this work.

Method	Obtained information	Studied materials	Publication
AFM	Surface morphology	La_2O_3	**II**
Electrical measurements	Permittivity and leakage current	ZrO_2	**III**
HTXRD	Crystallinity	La_2O_3	**II**
SEM	Surface morphology	Y_2O_3, ZrO_2, Gd_2O_3, PrO_x, Dy_2O_3	**I, III**
Spectrophotometer	Film thickness	Y_2O_3, La_2O_3, Gd_2O_3, PrO_x, Dy_2O_3	**I, II, IV**
TGA	Precursor evaporation and decomposition	Y_2O_3, ZrO_2, La_2O_3, Gd_2O_3, PrO_x, Dy_2O_3	**III**
TOF-ERDA	Impurities, stoichiometry	Y_2O_3, ZrO_2, La_2O_3, Gd_2O_3, PrO_x, Dy_2O_3	**I, II, III, IV**
XRD	Crystallinity	Y_2O_3, ZrO_2, La_2O_3, Gd_2O_3, PrO_x, Dy_2O_3	**I, II, III, IV**
XRR	Film thickness and density	Y_2O_3, ZrO_2, La_2O_3, Gd_2O_3, PrO_x, Dy_2O_3	**I, II, III**

7 Results and discussion

7.1 Precursor properties

The molecular structures of the metal precursors studied in this work are depicted in Figure 10. RE(^{i}PrCp)$_2$(^{i}Pr-amd) precursors were liquid whereas the zirconium precursors were solid. Zr(Cp)(^{t}BuDAD)(O^{i}Pr) and Zr(MeCp)(TMEA) melted in the reactor before deposition.

The thermogravimetric results of the RE(^{i}PrCp)$_2$(^{i}Pr-amd) precursors looked very similar to each other: evaporation in one step with low residues was observed for all the precursors. The highest residue (< 3 %) was observed for Gd(^{i}PrCp)$_2$(^{i}Pr-amd) (Figure 11). The TGA results indicate suitability of the precursors to ALD.

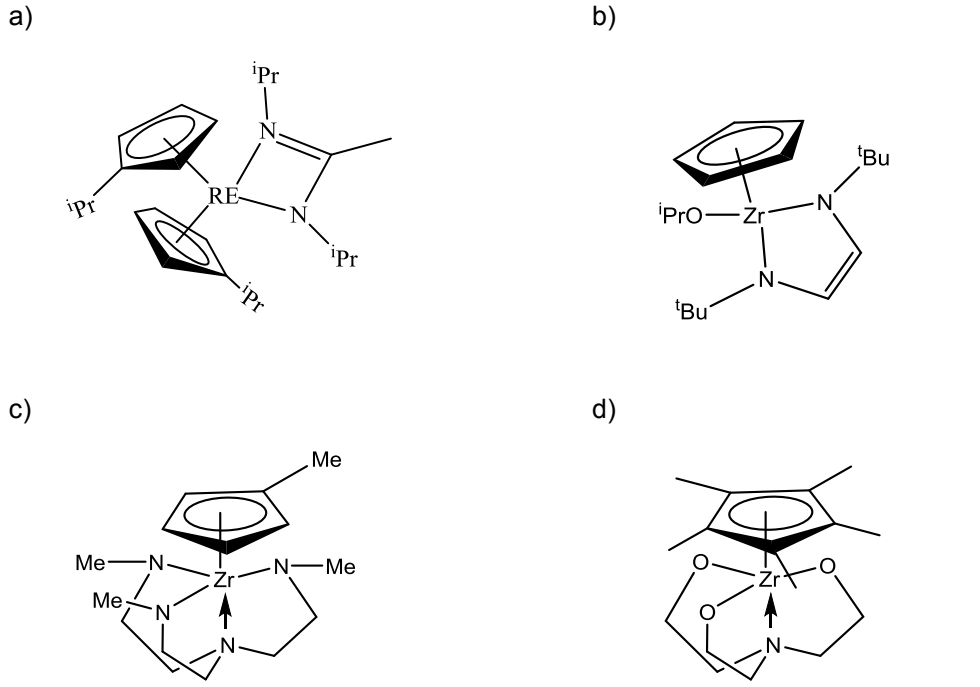

Figure 10. Molecular structures of the studied metal precursors. a) RE(^{i}PrCp)$_2$(^{i}Pr-amd) (RE = Y, La, Pr, Gd or Dy) b) Zr(Cp)(^{t}BuDAD)(O^{i}Pr) c) Zr(MeCp)(TMEA) d) Zr(Me$_5$Cp)(TEA).

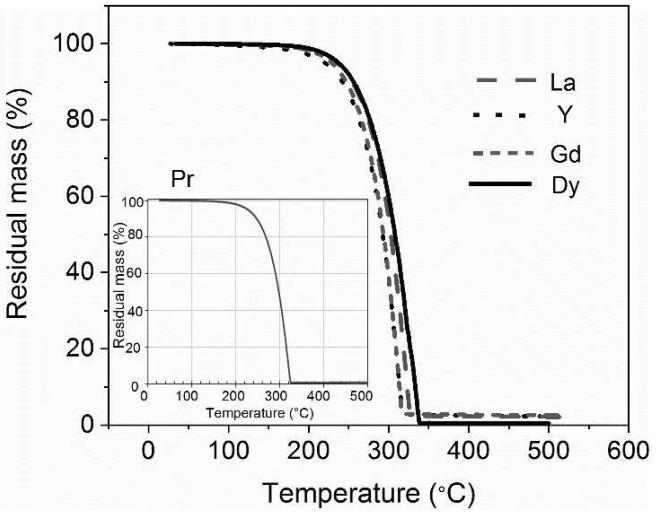

Figure 11. Thermogravimetric analysis of the RE(^{i}PrCp)$_2$(^{i}Pr-amd) precursors. The TG curve for Pr compound is shown in the inset for clarity.

The idea behind the studied zirconium compounds was to generate precursors that have at the same time high thermal stability and relatively good volatility. The TG curve for Zr(Cp)(^{t}BuDAD)(O^{i}Pr) showed evaporation with a residue of < 2 %. For the Zr(MeCp)(TMEA) precursor the residue was around 15 %. Zr(Me$_5$Cp)(TEA) showed two-step weight loss with 30 % residue when measured at atmospheric pressure. In vacuum the results were clearly better with a 15 % residue (Figure 12a). Although the TG measurements were not optimal for the Zr(Me$_5$Cp)(TEA) precursor, ALD experiments were successful and the first signs of decomposition were seen only at 400 °C, as there was coloration in the hot end of the precursor source tube that was not seen at lower temperatures. According to the vapor pressure data, Zr(Cp)(^{t}BuDAD)(O^{i}Pr) was clearly more volatile than the other two Zr precursors (Figure 12b). This was also seen in the source temperatures, as the Zr(Cp)(^{t}BuDAD)(O^{i}Pr) source temperature was 65 °C whereas the Zr(Me$_5$Cp)(TEA) and Zr(MeCp)(TMEA) source temperatures were 115 °C and 120 °C.

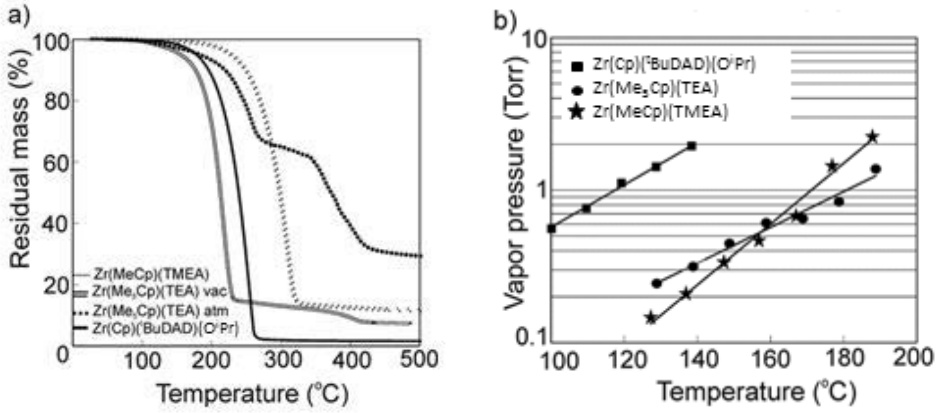

Figure 12. a) TG curves and b) vapor pressures of the Zr precursors.

7.2 Rare earth oxide depositions

7.2.1 La_2O_3 [II]

Good quality lanthanum oxide films have been difficult to deposit by ALD because there are problems with the both most common oxygen sources, H_2O and O_3. As discussed in Chapter 4, the hygroscopicity of the La_2O_3 film destroys the important feature of ALD, the self-limiting growth, and causes very high growth rates with thickness nonuniformity when water is used as the oxygen source.[43] With ozone, the problem is high carbon impurity levels caused by carbonate formation.[19] Because of the issues related to O_3 and H_2O, also alternative oxygen sources were tested in this work. These were ethanol as well as water and ozone in the same deposition process. In the latter approach, the pulsing sequence was following: La(^{i}PrCp)$_2$(^{i}Pr-amd) pulse-purge-H_2O pulse-purge-O_3 pulse-purge.

High growth rates were observed with the La(^{i}PrCp)$_2$(^{i}Pr-amd)/H_2O process. Different purge lengths after the water pulses were studied and the growth rates decreased considerably with increasing purge length (Figure 13). However, saturation of the growth rate could not be achieved even with 20 s long purges.

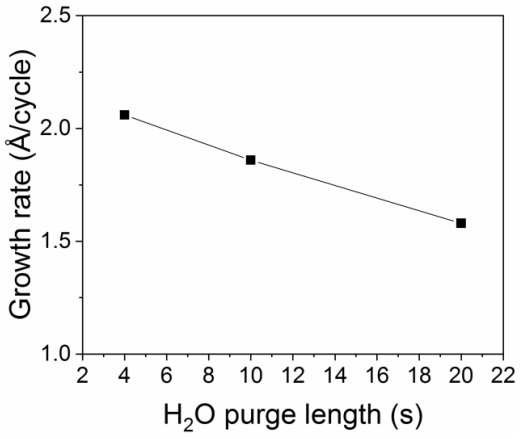

Figure 13. La_2O_3 growth rate as a function of H_2O purge length at 200 °C. The La(^{i}PrCp)$_2$(^{i}Pr-amd) precursor pulse and purge times were 1.0 s and 1.5 s and H_2O pulse 1.0 s.

With ozone, self-limiting growth was obtained at 200 and 225 °C (Figure 14). These films were amorphous and contained high levels of carbon impurities. However, in situ high temperature XRD studies in N_2 atmosphere showed that it is possible to crystallize the films to either the cubic or hexagonal La_2O_3 phase by tuning the annealing temperature (Figure 15a).

The approach of using both water and oxygen in the same deposition process proved to be successful. The carbon impurities caused by the ozone pulses suppressed the hygroscopicity of the film and shorter purge time after the water pulses could be used: the growth rate did not decrease when the purge time was doubled from 10 to 20 s. On the other hand, these films did not have as high carbon impurity levels as the films deposited with ozone as the only oxygen source. Saturation was achieved at 200 °C (Figure 14). Like with ozone, these films were amorphous, and the final phase could be tuned by annealing in N_2 atmosphere (Figure 15b).

The films deposited above 200 °C with the La(^{i}PrCp)$_2$(^{i}Pr-amd)/H_2O/O_3 process were cubic La_2O_3. Interestingly, annealing in air at 700 °C turned all the films deposited at 250 – 325 °C to the hexagonal La_2O_3, whereas with ozone as the only oxygen source, mixtures of the cubic and hexagonal phases were obtained after annealing the films deposited at 250 – 325 °C. With water, a mixture of the phases was observed in films deposited at 200 °C whereas only the hexagonal phase was detected in the films deposited above 200 °C.

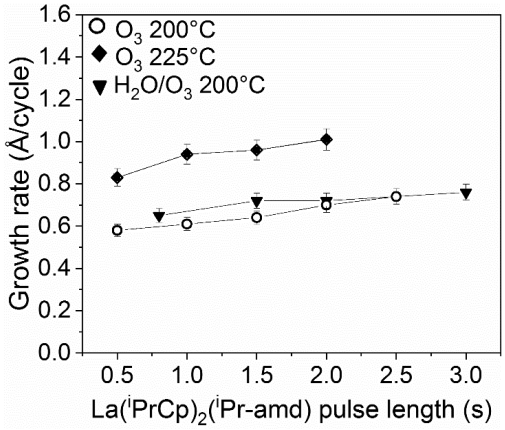

Figure 14. La_2O_3 film growth rate as a function of La(^{i}PrCp)$_2$(^{i}Pr-amd) pulse length. Pulse time for H_2O was 0.8 s and for O_3 1.0 s.

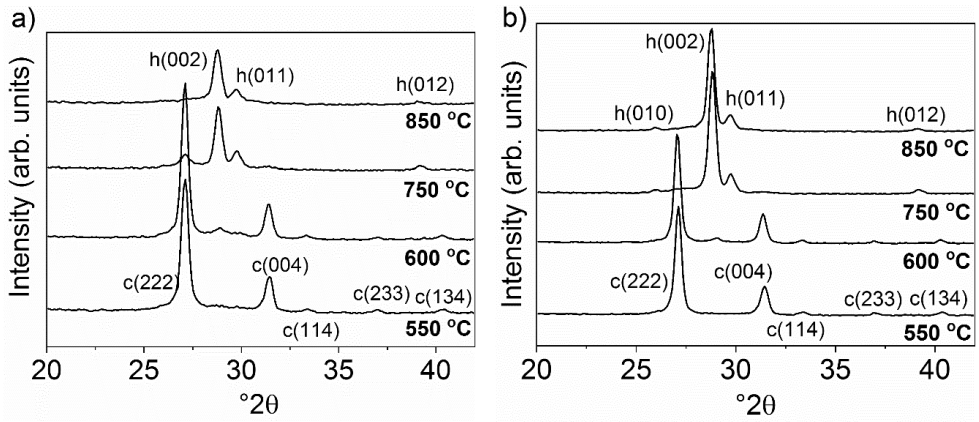

Figure 15. HTXRD patterns of the La_2O_3 films deposited at 200 °C with a) O_3 and b) H_2O/O_3 measured in N_2 atmosphere.[II]

Ethanol was tested as an oxygen source for the deposition of La_2O_3 to see if it has a lower reactivity toward the $La(OH)_3$ formation than water. At 200 – 275 °C, the growth rates resembled the growth rates of the films deposited with O_3 or H_2O/O_3 as the oxygen source. However, at 300 °C the growth rate increased considerably, to the same level as with water at 300 °C (Figure 16). The clearly higher growth rate at 300 °C could be caused by ethanol dehydration that produces water and leads to CVD-type reactions. It has been reported before that metal oxide surfaces are catalytically active towards alcohol dehydration reactions.[162,163] Also, the TOF-ERDA depth profile showed high hydrogen concentration throughout the whole thickness of a film deposited at 300 °C whereas at lower deposition temperatures the hydrogen concentration was the highest on the surface and decreased deeper in the film (Figure 17). However, self-limiting growth was not observed at any deposition temperature with ethanol.

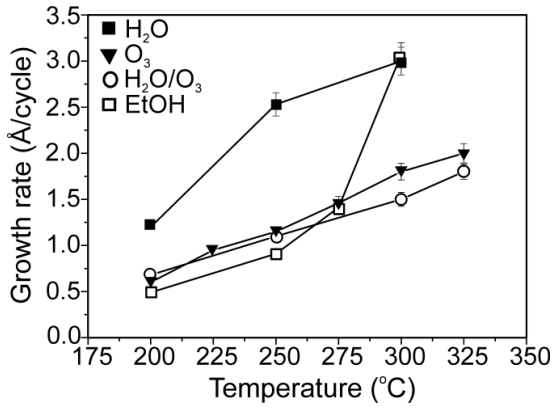

Figure 16. Growth rates of the La_2O_3 films at different temperatures deposited with La(^{i}PrCp)$_2$(^{i}Pr-amd)/H_2O (0.8 s precursor pulses, 20 s purge after H_2O), La(^{i}PrCp)$_2$(^{i}Pr-amd)/O_3 (1.0 s pulses), La(^{i}PrCp)$_2$(^{i}Pr-amd)/H_2O/O_3 (0.8 s La and H_2O pulses, 1.0 s O_3 pulse, 10 s purge after H_2O), and La(^{i}PrCp)$_2$(^{i}Pr-amd)/EtOH processes (0.7 s pulses).[II]

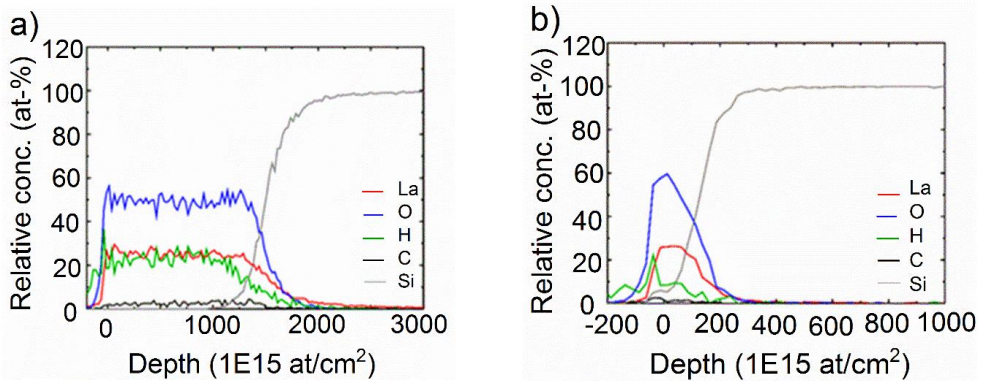

Figure 17. TOF-ERDA depth profiles of the films deposited with the La(^{i}PrCp)$_2$(^{i}Pr-amd)/EtOH process at a) 300 °C and b) 200 °C.

In the films deposited with ethanol, XRD revealed mixtures of either cubic La_2O_3 and $La(OH)_3$ or hexagonal La_2O_3 and $La(OH)_3$ depending on the deposition temperature. Annealing in air at 700 °C did not remove all the hydroxyl species from the films deposited at 200 and 250 °C since LaO(OH) peaks were identified in addition to La_2O_3 peaks from the x-ray diffractograms measured after the annealing. In contrast, the film deposited at 300 °C was hexagonal La_2O_3 after the annealing.

There are not many successful La_2O_3 ALD processes reported in literature. The same problems as reported before with ozone and water could be seen in this study too. The combination of separate O_3 and H_2O pulses as the oxygen source suppressed the poor features of the processes using ozone or water alone.

7.2.2 PrO_x[I, IV]

Praseodymium oxide suffers from the same problem with hygroscopicity as La_2O_3. Accordingly, praseodymium oxide films have so far been very difficult to deposit with ALD. Self-limiting growth has been reported only for the $Pr(EtCp)_3/H_2O$ process at 130 °C.[79]

Similar to the $La(^iPrCp)_2(^iPr\text{-}amd)/H_2O$ process, decreasing growth rate with increasing H_2O purge length was observed with the $Pr(^iPrCp)_2(^iPr\text{-}amd)/H_2O$ process. Uniform films were deposited at 200 °C but saturation was not quite achieved as the growth rate increased from 0.9 Å/cycle with 0.5 s pulses to 1.1 Å/cycle with 1.5 s pulses (Figure 18a). Different from the La_2O_3 deposition, Pr_2O_3 growth rate was nearly constant throughout the studied temperature range of 200 – 300 °C (Figure 18b). XRD results confirmed the films to be mainly cubic Pr_2O_3 with a couple of small peaks attributed to the hexagonal Pr_2O_3. Although self-limiting growth was not achieved, good quality, uniform films could be deposited making this process one of the best among the small group of ALD processes for praseodymium oxide films.

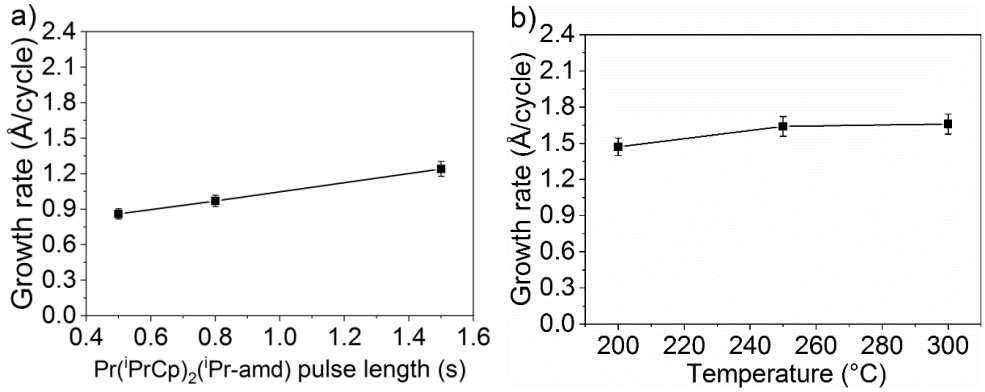

Figure 18. a) Pr_2O_3 growth rate versus Pr precursor pulse length at a deposition temperature of 200 °C with a 0.8 s water pulse and a 20 s purge b) Pr_2O_3 growth rates at 200−300 °C for $Pr(^iPrCp)_2(^iPramd)/H_2O$ with 0.8 s pulses, 4.0 s purge after the Pr precursor pulse, and 8.0 s purge after the H_2O pulse. [1]

$Pr(^iPrCp)_2(^iPr\text{-}amd)$ together with ozone produced highly nonuniform films and it was impossible to measure the film thicknesses. For this reason, only a few films were deposited with this process. The nonuniformity of the films deposited with ozone has also been reported by Hansen et al. when using $Pr(thd)_3$ and O_3. They explained it by the catalytic activity of praseodymium oxide rising from the mixed oxidation states of praseodymium caused by the strong oxidant ozone.[49] From the rare earth elements studied in this thesis, Pr is the only one that has two possible oxidation states (+III and +IV) under the deposition conditions. Indeed, the other rare earth oxides did not exhibit thickness gradients similar to praseodymium oxide when deposited with ozone.

XRD measurements showed that the films deposited at 200 °C were crystalline. However, the peaks were so broad that the phase of the films could not be distinguished. Possible phases are Pr_6O_{11} and PrO_2.

7.2.3 Gd_2O_3 [I, IV]

Self-limiting growth was achieved with the $Gd(^iPrCp)_2(^iPr\text{-}amd)/O_3$ process at 200 and 225 °C with growth rates of 0.4 and 0.8 Å/cycle (Figure 19a). These films were amorphous with high carbon contents. Carbon contamination clearly decreased with increasing deposition temperature, from 15 at. % at 200 °C to 3 at. % at 300 °C. Cubic Gd_2O_3 films were deposited at 300 °C and mixtures of cubic and monoclinic phases at higher deposition temperatures. Annealing in air at 700 °C decreased the carbon contamination and for example the carbon content of a film deposited at 250 °C was 1.7 at. % after the annealing. High carbon content and excess oxygen due to carbonate type impurities have been reported also for the $Gd(thd)_3/O_3$ process.[51] The main advantage of the $Gd(^iPrCp)_2(^iPr\text{-}amd)/O_3$ process over the $Gd(thd)_3/O_3$ process is the higher growth rate: at 225 °C the growth rate is 0.8 Å/cycle whereas the growth rate of the $Gd(thd)_3/O_3$ process is 0.3 Å/cycle at 300 °C.

With water, both short (1.5 s) and long (20 s) purges after the water pulses were tested at 200 °C. Saturation of the growth rate was not quite achieved even with the long purge time (Figure 19b). However, the film thickness followed linearly the cycle number and uniform films with the cubic Gd_2O_3 phase and a carbon content around 1 at. % were obtained. With a homoleptic $Gd(MeCp)_3$ precursor, results similar to ours were reported when it was used together with water: no saturation but uniform films with low carbon contents.[51] In this regard, the heteroleptic Cp-amidinate precursor does not bring advantage over the homoleptic one when water is used as the oxygen source.

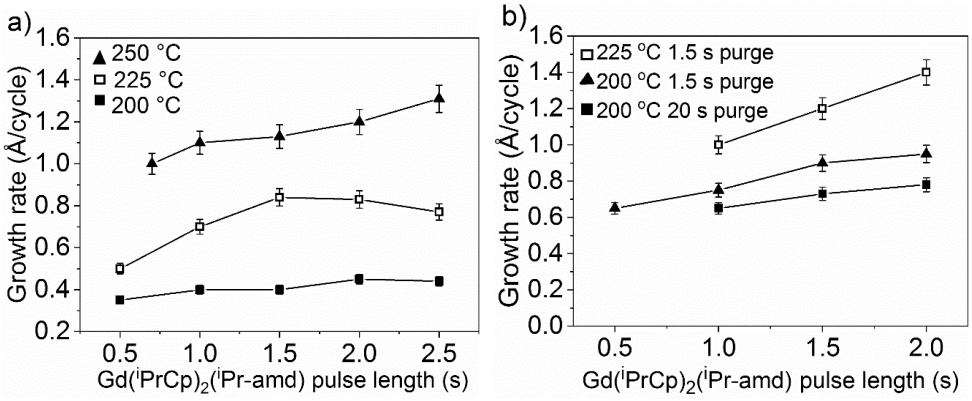

Figure 19. Gd_2O_3 growth rates as a function of $Gd(^iPrCp)_2(^iPr\text{-}amd)$ precursor pulse length with a) ozone and b) water as the oxygen source. Pulse times for O_3 and H_2O were 1.0 s and O_3 purge 1.5 s.

7.2.4 Y_2O_3 [I, IV]

$Y(^iPrCp)_2(^iPr\text{-}amd)$ resulted in self-limiting growth with both oxygen sources at as high temperature as 350 °C with a growth rate of 1.2 Å/cycle with O_3 and 1.1 Å/cycle with H_2O (Figure 20). Clearly, $Y(^iPrCp)_2(^iPr\text{-}amd)$ was thermally the most stable of the Cp-amd precursors examined. From the other Y_2O_3 ALD processes studied, only the $Y(thd)_3/O_3$ process saturates at this high temperature, but it has a growth rate of only 0.23 Å/cycle. The XRD results were similar to the La_2O_3 and Gd_2O_3 results in that crystalline films could be deposited with water at 200 °C whereas with ozone 300 °C was needed. The crystalline Y_2O_3 films deposited with ozone were cubic. The $Y(^iPrCp)_2(^iPr\text{-}amd)/H_2O$ process produced mainly cubic films with a few very small peaks designated to the monoclinic Y_2O_3 phase (Figure 21).

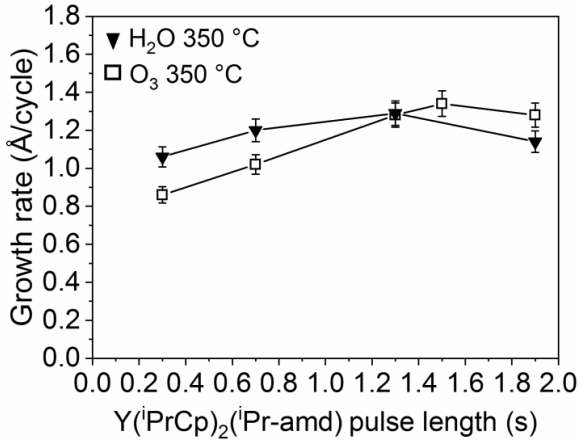

Figure 20. Y_2O_3 growth rate saturation at 350 °C.[I]

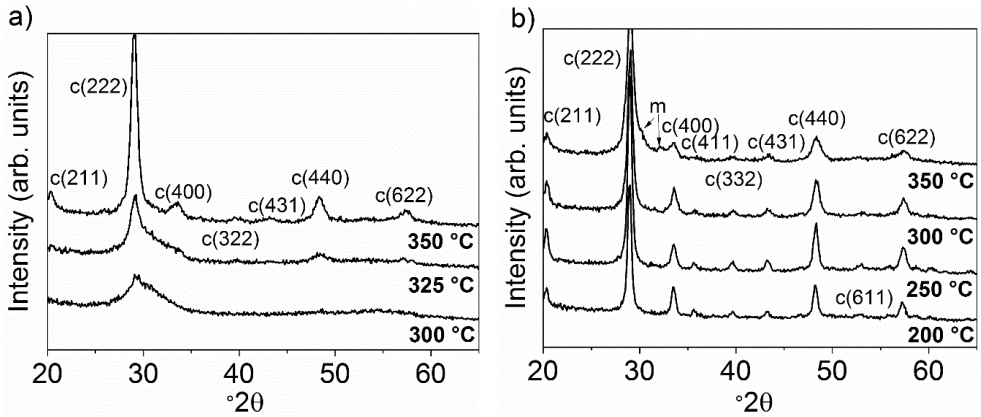

Figure 21. X-ray diffractograms of Y_2O_3 films deposited at different temperatures with a) ozone and b) water as the oxygen source.[I]

Compared to the homoleptic Y(^{i}Pr-amd)$_3$, the thermal stability of the heteroleptic Y(^{i}PrCp)$_2$(^{i}Pr-amd) is considerably higher: saturation was achieved with the Y(^{i}Pr-amd)$_3$/H_2O process at 280 °C with a growth rate of 0.8 Å/cycle.[65] With homoleptic Cp precursors, YCp_3 and Y(MeCp)$_3$, self-limiting growth has been verified at 300 °C.[70]

7.2.5 Dy_2O_3 I

Growth rates of the Dy_2O_3 films were similar to the growth rates of the Y_2O_3 films, especially at low deposition temperatures. Saturation was studied with water as the oxygen source at 300 °C and with ozone at 300 and 325 °C. With water, the growth rate was 1.3 Å/cycle with short Dy precursor pulse lengths but increased to 1.9 Å/cycle with longer pulse lengths. With ozone, the growth rate increased only moderately from 1.0 to 1.2 Å/cycle when the Dy(^{i}PrCp)$_2$(^{i}Pr-amd) pulse length was increased from 0.7 and 1.3 s to 1.9 s (Figure 22). There are not many Dy precursors for the ALD of Dy_2O_3. The Dy(DPDMG)$_3$/H_2O process has been reported to exhibit saturative growth at 250 °C with a growth rate of 1.0 Å/cycle.[63] Dy(thd)$_3$ has been tested with ozone at 300 °C and the growth rate was quite low, 0.3 Å/cycle.[49]

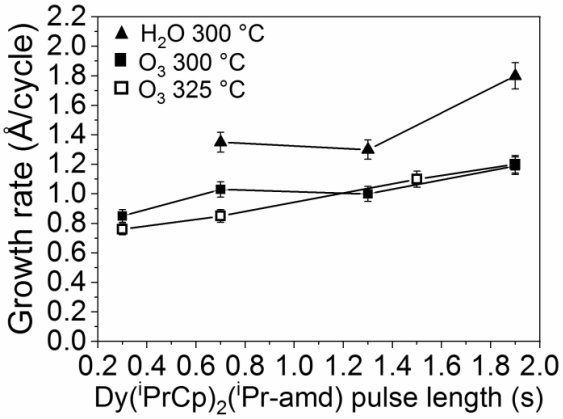

Figure 22. Dy_2O_3 growth rate saturation studies with Dy(^{i}PrCp)$_2$(^{i}Pr-amd)/H_2O and Dy(^{i}PrCp)$_2$(^{i}Pr-amd)/O_3 processes. H_2O and O_3 pulses were 1.0 s and purge times 1.5 s.

7.2.6 Summary on the RE oxide studies

Self-limiting growth, the key feature of ALD, was achieved with the Y(^{i}PrCp)$_2$(^{i}Pr-amd)/H_2O, Y(^{i}PrCp)$_2$(^{i}Pr-amd)/O_3, La(^{i}PrCp)$_2$(^{i}Pr-amd)/O_3, La(^{i}PrCp)$_2$(^{i}Pr-amd)/H_2O/O_3, and Gd(^{i}PrCp)$_2$(^{i}Pr-amd)/O_3 processes (Figure 23a). Self-limiting growth could not be reached with the Pr and Dy precursors with neither water nor ozone. However, the Dy(^{i}PrCp)$_2$(^{i}Pr-amd)/O_3 process at 300 °C and the Pr(^{i}PrCp)$_2$(^{i}Pr-amd)/H_2O process at 200 °C produced uniform films and the increase of the growth rate with increasing pulse lengths was moderate (Figure 23b). The key results are collected in Table 8. In all the studied rare earth oxide processes, the films deposited with water were crystalline at a deposition temperature of 200 °C whereas with ozone at least 300 °C was needed for proper diffraction peaks to

appear. PrO_x made an exception since also the films deposited with ozone were crystalline at 200 °C. The reason for the high crystallization temperatures is most likely the high carbon contents of the films deposited at low temperatures with ozone that disturbs the crystallization. In this study, very high carbon contents at low deposition temperature were confirmed for La_2O_3 and Gd_2O_3 films when ozone was used as the oxygen source. The carbon content of Gd_2O_3 films decreased from 15 at% to 3 at% when deposition temperature was increased from 200 to 300 °C. In the case of La_2O_3, the carbon content was 19 at% at 200 °C and 4 at% at 325 °C.

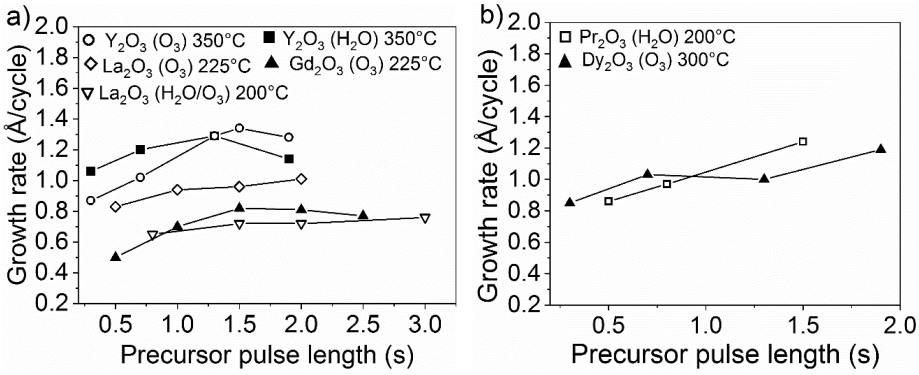

Figure 23. a) Self-limiting growth processes for Y_2O_3, La_2O_3 and Gd_2O_3 and b) best processes for Pr_2O_3 and Dy_2O_3.

Table 8. Growth rates at optimal temperatures and summary of the crystallinities of the films deposited by the studied RE oxide processes.

Process	Saturation temp. (°C)	GR at T_{sat} or T_{best} (Å/cycle)	Crystallinity
Y(^{i}PrCp)$_2$(^{i}Pr-amd)/H_2O	350	1.2	*c* Y_2O_3, at high T also small *m* peaks
Y(^{i}PrCp)$_2$(^{i}Pr-amd) /O_3	350	1.3	*c* Y_2O_3 above 300 °C, amorphous below
La(^{i}PrCp)$_2$(^{i}Pr-amd)/H_2O	-	1.2 (200 °C)*	Mixture of *c* and *h* La_2O_3
La(^{i}PrCp)$_2$(^{i}Pr-amd)/O_3	225	1.0	*a,* at low T, *c* La_2O_3 at 300 °C, above mixture of *c* and *h* La_2O_3
La(^{i}PrCp)$_2$(^{i}Pr-amd) /H_2O/O_3	200	0.7	*c* La_2O_3 at 300 °C and above, amorphous below
La(^{i}PrCp)$_2$(^{i}Pr-amd) /EtOH	-	-	Mainly $La(OH)_3$ at low T, at 300 °C $La(OH)_3$ and h La_2O_3
Pr(^{i}PrCp)$_2$(^{i}Pr-amd)/H_2O	-	0.9-1.2 (200 °C)	*c* or mixture of *c* and *h* Pr_2O_3 depending on temperature
Pr(^{i}PrCp)$_2$(^{i}Pr-amd)/O_3	-	Could not be measured	*c* Pr_6O_{11} or PrO_2
Gd(^{i}PrCp)$_2$(^{i}Pr-amd)/H_2O	-	0.65-0.78 (200 °C)	*c* Gd_2O_3 at 200 °C, mainly *m* Gd_2O_3 above
Gd(^{i}PrCp)$_2$(^{i}Pr-amd)/O_3	250	1.2	*c* Gd_2O_3 at 300 °C, *c* and *m* Gd_2O_3 above
Dy(^{i}PrCp)$_2$(^{i}Pr-amd)/H_2O	-	1.4 (300 °C)	*c* Dy_2O_3
Dy(^{i}PrCp)$_2$(^{i}Pr-amd)/O_3	-	0.9-1.2 (300 °C)	*c* Dy_2O_3 above 300 °C

* with 0.8 s precursor pulses and 20 s purge after water pulse

7.3 Zirconium oxide depositions [III]

7.3.1 Zr(Me_5Cp)(TEA)

With the Zr(Me_5Cp)(TEA)/O_3 process, self-limiting growth was confirmed at 300, 350 and 375 °C (Figure 24). The growth rates were 0.30 Å/cycle at 300 °C and 0.40 Å/ cycle at 350 and 375 °C. The resulting film purity was excellent at all these temperatures, as the carbon, hydrogen and nitrogen levels were even below the detection limit (0.1 at.%) of TOF-ERDA. 375 °C is the highest saturation temperature that has been achieved with the advanced heteroleptic Zr precursors and it is clearly higher than the saturation temperature reported for the widely used zirconium precursors heteroleptic CpZr(NMe_2)$_3$ (300 °C) and homoleptic Zr(NEtMe)$_4$ (below 300 °C).[114,115] From the homoleptic precursors, $ZrCl_4$ has been reported to have higher saturation temperatures.

With water, 400 °C was needed to attain any growth at all. The growth rate was very low, only 0.1 Å/cycle with 1.0 s Zr precursor pulse and increased to 0.2 Å/cycle with 3.5 s pulse (Figure 24). At 425 °C, the growth rate was 0.2 Å/cycle but decomposition of the Zr precursor was already seen at that temperature. The film densities obtained from the XRR measurements showed that the densities of the films deposited with water were far from bulk densities, only 4.7 g/cm^3 whereas the bulk density is around 6 g/cm^3. Because of the low growth rates and film densities, only a few films were deposited with the $Zr(Me_5Cp)(TEA)/H_2O$ process and they were not fully characterized. With ozone, the film densities were 5.8 – 5.9 g/cm^3. The film thickness did not affect the density and also the thinnest films around 10 nm in thickness had density comparable to the thicker films.

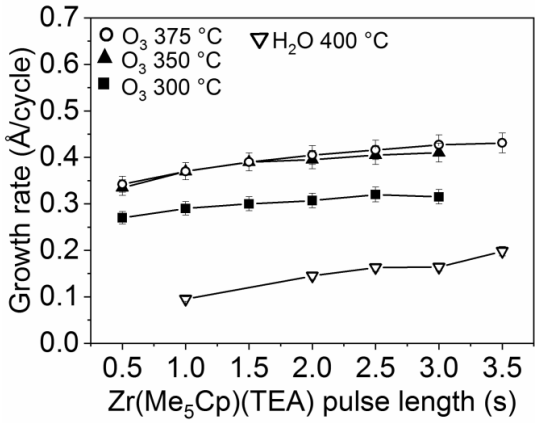

Figure 24. ZrO_2 growth rate saturation studies at different deposition temperatures. Pulse lengths for water and ozone were 1.0 s and purge lengths 1.5 s.

The crystalline phase of the films deposited with the $Zr(Me_5Cp)(TEA)/O_3$ process varied with deposition temperature and film thickness. At low temperatures, only the tetragonal ZrO_2 phase was seen in XRD. The intensities of the monoclinic diffraction peaks increased with increasing temperature, but the tetragonal phase remained the dominant one assessed from the peak intensities. Very thin films were tetragonal also at higher deposition temperatures (Figure 25). All the films deposited with water as the oxygen source were tetragonal ZrO_2.

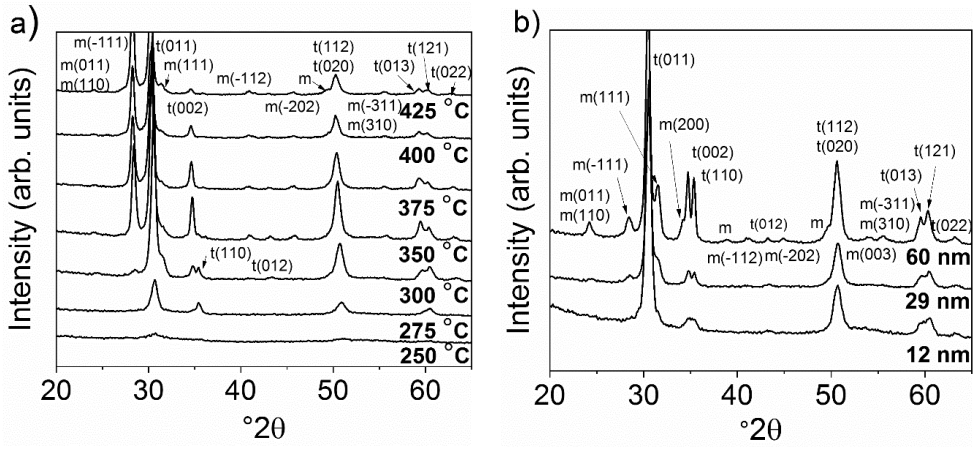

Figure 25. X-ray diffractograms of the films deposited with a) $Zr(Me_5Cp)(TEA)/O_3$ process at 250 – 425 °C and b) $Zr(Me_5Cp)(TEA)/O_3$ process at 300 °C with different film thicknesses. In a) the film thicknesses varied between 29 and 40 nm.

The dielectric constants of the films deposited at 300 – 375 °C with the $Zr(Me_5Cp)(TEA)/O_3$ process decreased from 29 to 24 when the deposition temperature was increased from 300 to 375 °C. This decrease could be due to the higher amount of the lower dielectric constant monoclinic ZrO_2 phase at higher deposition temperatures. Previously, dielectric constants between 20 and 40 have been reported for tetragonal/cubic ZrO_2 films by ALD. Low leakage currents in the order of 10^{-8} A/cm^2 at 1 MV/cm field were measured for all studied films (Figure 26).

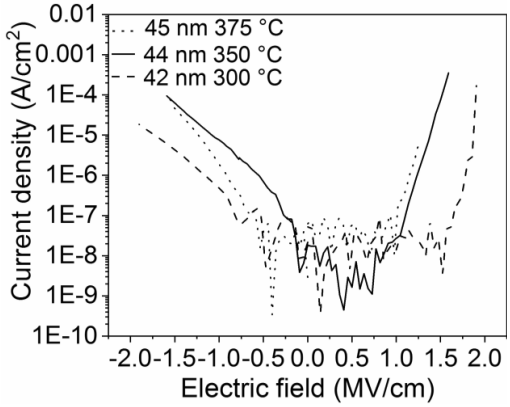

Figure 26. Leakage current densities for films deposited at 300 – 375 °C with the $Zr(Me_5Cp)(TEA)/O_3$ process**.**

7.3.2 Zr(Cp)(^{t}BuDAD)(O^{i}Pr)

With Zr(Cp)(^{t}BuDAD)(O^{i}Pr), deposition studies were carried out at 250 – 375 °C with ozone and at 250 – 425 °C with water as the oxygen source. Film densities varied considerably with the deposition temperature, especially with water (Figure 27). Self-limiting growth was verified at 250 °C with the Zr(Cp)(^{t}BuDAD)(O^{i}Pr)/O_3 process. The growth rate was 0.40 Å/cycle (Figure 28). However, the film densities at this low temperature were somewhat lower than the bulk value, 5.1 g/cm^3. The main impurities at 250 °C were hydrogen and carbon, but their concentrations were quite low, around 1 at-%. Saturation of the growth rate was not achieved with water (Figure 28), but tetragonal ZrO_2 films could be deposited at as high temperature as 375 °C with a film thickness ranging from 9 to 70 nm (Figure 29). With ozone at 250 °C at least 50 nm thick films and below were tetragonal ZrO_2, whereas at 300 °C small monoclinic peaks were visible in XRD of already a 9 nm thick film.

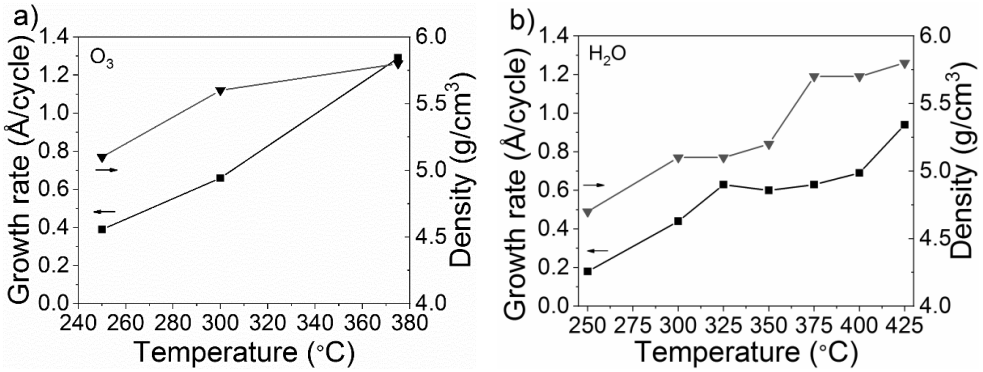

Figure 27. Growth rates and densities of ZrO_2 films deposited at a) 250 – 375 °C with Zr(Cp)(^{t}BuDAD)(O^{i}Pr)/O_3 and b) at 250 – 425 °C with Zr(Cp)(^{t}BuDAD)(O^{i}Pr)/H_2O process. Pulses were 1.0 s and purges 1.5 s.

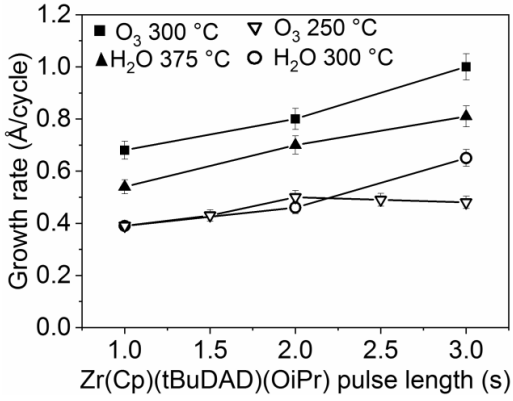

Figure 28. Growth rate saturation tests with water or ozone as the oxygen source. O_3 and H_2O pulses were 1.0 s.

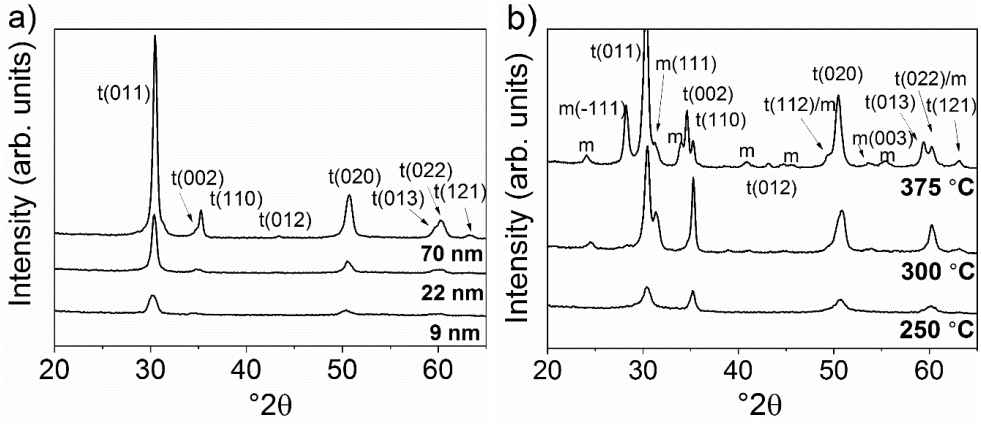

Figure 29. a) X-ray diffractograms of ZrO_2 films with different thicknesses deposited with the Zr(Cp)(^{t}BuDAD)(O^{i}Pr)/H_2O process at 375 °C. b) Diffractograms of ZrO_2 films deposited with the Zr(Cp)(^{t}BuDAD)(O^{i}Pr)/O_3 process at different temperatures. Film thicknesses in b) are 47 nm (250 °C), 54 nm (300 °C) and 96 nm (375 °C).

Leakage current densities were in the range of 10^{-8} – 10^{-7} A/cm^2 at 1.0 MV/cm field for most samples deposited at 300 – 375 °C. The film deposited with water at 300 °C had clearly higher leakage current density of 1×10^{-5} A/cm^2 (Figure 30). No obvious reason for this result could be found.

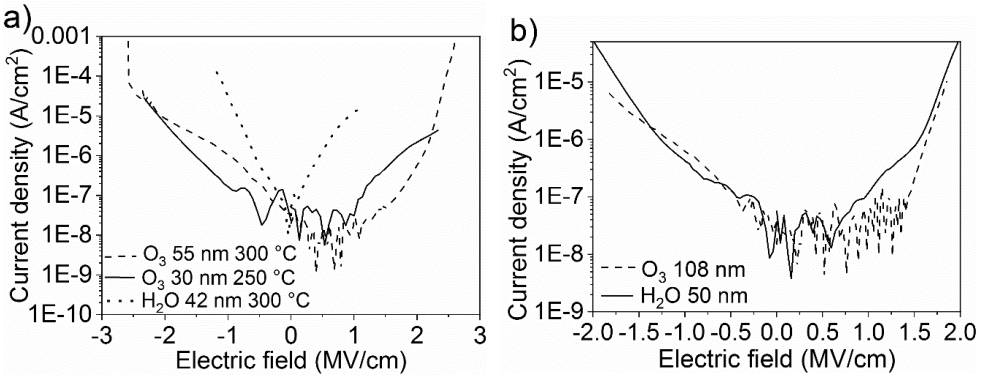

Figure 30. Leakage current densities of ZrO_2 films deposited at a) 250 and 300 °C and b) 375 °C.

7.3.3 Zr(MeCp)(TMEA)

Growth rates of the films deposited with the Zr(MeCp)(TMEA)/O_3 and Zr(MeCp)(TMEA)/H_2O processes were studied at 200 – 375 °C (Figure 31). With ozone the growth rate decreased from 0.65 Å/cycle at 200 °C to 0.51 Å/cycle at 375 °C. However, significant densification of the film occurred with increasing deposition temperature, from 3.6 g/cm^3 to 5.8 g/cm^3, meaning that the amount of material deposited at 350 and 375 °C is actually higher than at 250 and 300 °C even though the growth rate decreased (Figure 31a). With water, the growth rate slightly increased with increasing deposition temperature, from 0.23 to 0.33 Å/cycle. Film densification was also observed with water as the oxygen source (Figure 31b). Uniform films could be deposited with the Zr(MeCp)(TMEA)/O_3 and Zr(MeCp)(TMEA)/H_2O processes but full saturation was not achieved in either case (Figure 32).

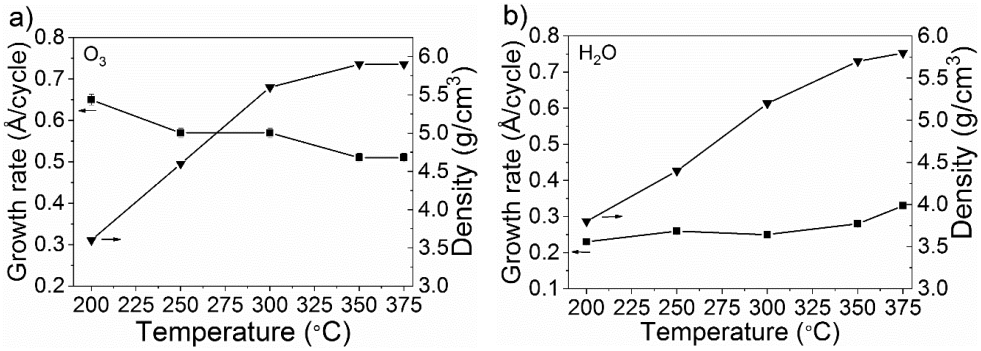

Figure 31. Growth rates and film densities for a) Zr(MeCp)(TMEA)/O_3 and b) Zr(MeCp)(TMEA)/H_2O processes.

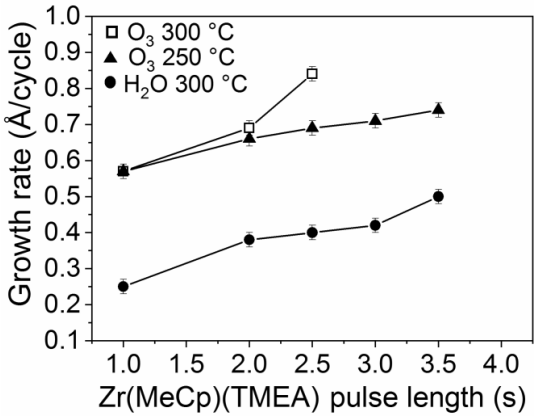

Figure 32. ZrO_2 film growth rates as a function of the Zr(MeCp)(TMEA) pulse length. Ozone and water pulses were 1.0 s and purges 1.5 s.

As with the other studied zirconium precursors, the deposition temperature as well as the film thickness affected the crystalline phase of the films. The tetragonal ZrO_2 phase was the dominating one but the intensity of the monoclinic peaks increased with increasing temperature (Figure 33). The leakage current densities of the films deposited with ozone were 1 – 2 orders of magnitude higher than with the other zirconium precursors depending on the deposition temperature and varying from 6×10^{-6} to 2×10^{-7} A/cm^2 at 1 MV/cm. With water, the leakage currents were in the same range as with ozone (Figure 34).

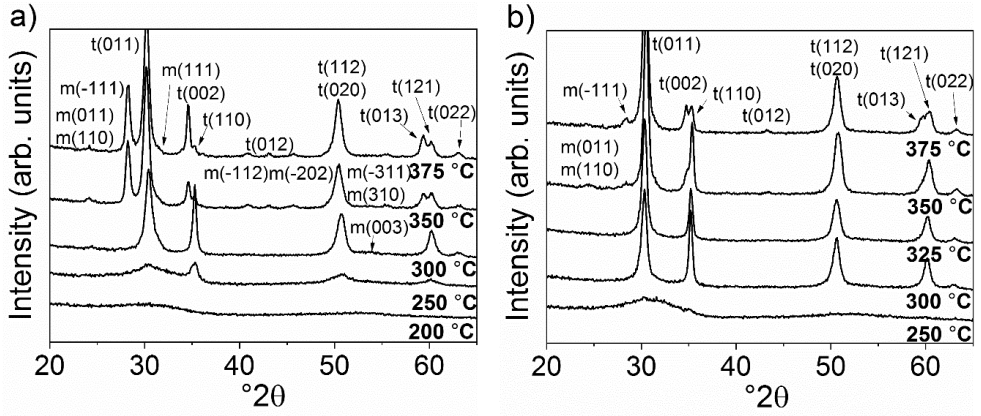

Figure 33. Diffractograms of ZrO_2 films deposited with a) Zr(MeCp)(TMEA)/O_3 process (film thickness 40 – 52 nm) and b) Zr(MeCp)(TMEA)/H_2O process (43 – 51 nm).

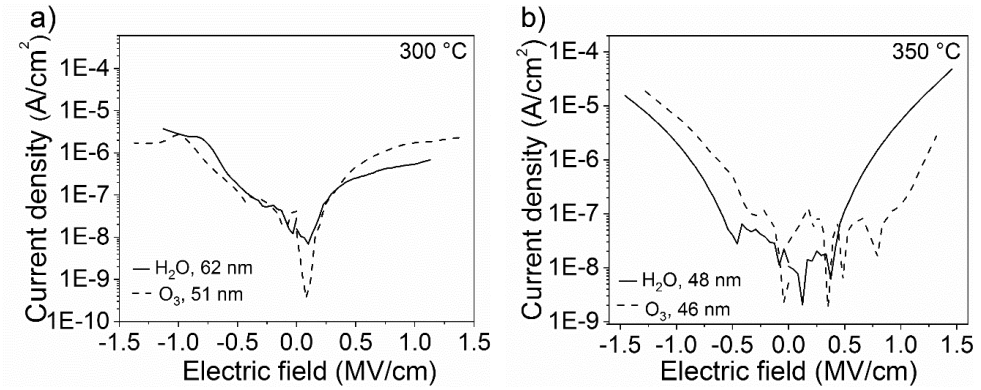

Figure 34. Leakage current densities of ZrO_2 films deposited at a) 300 °C and b) 350 °C with the Zr(MeCp)(TMEA)/O_3 and Zr(MeCp)(TMEA)/H_2O processes.

7.3.4 Summary of the ZrO_2 studies

Three new Zr precursors were evaluated for the ALD of ZrO_2. $Zr(Me_5Cp)(TEA)$ was found to be the best one showing high thermal stability and depositing films with high density and very low impurity contents at the saturation temperature of 300 – 375 °C with ozone as the oxygen source. The exceptionally high thermal stability is apparently due to the chelating four-dentate TEA ligand with three oxygen atoms and one nitrogen atom as donors. For the same reason the reactivity of $Zr(Me_5Cp)(TEA)$ with water was poor. The high degree of substitution on the Cp ring with electron donor groups can also increase thermal stability of the precursor by strengthening the bond between the metal and the Cp ring. $Zr(Cp)(^tBuDAD)(O^iPr)/O_3$ process also showed self-limiting growth but at much lower temperature of 250 °C. At this temperature the impurity levels were low, but also the film density was low. With all three precursors both film thickness and deposition temperature affected the crystalline phase of the films. The effect of the film thickness on the phase was much stronger with ozone than with water. Very low leakage currents in the order of 10^{-8} A/cm^2 were obtained with the $Zr(Me_5Cp)(TEA)/O_3$ and $Zr(Cp)(^tBuDAD)(O^iPr)/O_3$ processes. Table 9 summarizes the growth rates and crystalline phases of the films deposited with the studied processes.

Table 9. Growth rates and crystallinity of the studied ZrO_2 processes.

Process	Saturation temp. (°C)	GR at T_{sat} or T_{best} (Å/cycle)	Crystallinity
$Zr(Me_5Cp)(TEA)/O_3$	300-375	0.3-0.4	*t* ZrO_2 or mixtures of *t* and *m* depending on T and film thickness
$Zr(Me_5Cp)(TEA)/H_2O$	-	0.1 (400 °C)	*t* ZrO_2
$Zr(Cp)(^tBuDAD)(O^iPr)/O_3$	250	0.5	*t* or mixture of *t* and *m* ZrO_2
$Zr(Cp)(^tBuDAD)(O^iPr)/H_2O$	-	0.5 (375 °C)	*t* ZrO_2 or mixtures of *t* and *m* depending on T and film thickness
$Zr(MeCp)(TMEA)/O_3$	-	0.65 (250 °C)	mixture of *t* and *m* ZrO_2
$Zr(MeCp)(TMEA)/H_2O$	-	0.4 (300 °C)	*t* or mixture of *t* and *m* ZrO_2

8 Conclusions

In this thesis work, new heteroleptic metal precursors were studied and processes for atomic layer deposition of rare earth oxides and zirconium oxide were developed. Rare earth oxides and zirconium oxide have great potential in several fields of applications including microelectronics, catalysis and energy. Various heteroleptic precursors, where the ligands in the compound are of at least two different types, have been studied for the ALD of ZrO_2 whereas only a few heteroleptic precursors have been studied for the rare earth oxide deposition.

Rare earth precursors RE(^{i}PrCp)$_2$(^{i}Pr-amd) (RE = Y, La, Pr, Gd and Dy) were studied to deposit Y_2O_3, La_2O_3, PrO_x, Gd_2O_3 and Dy_2O_3 thin films by ALD. Deposition processes with self-limiting growth were developed for Y_2O_3, La_2O_3, and Gd_2O_3. The Y(^{i}PrCp)$_2$(^{i}Pr-amd) precursor showed self-limiting growth with both water and ozone as the oxygen source at a high deposition temperature of 350 °C whereas La(^{i}PrCp)$_2$(^{i}Pr-amd)/O_3, La(^{i}PrCp)$_2$(^{i}Pr-amd)/H_2O/O_3 and Gd(^{i}PrCp)$_2$(^{i}Pr-amd)/O_3 processes saturated at 200 – 225 °C. Uniform Pr_2O_3 and Dy_2O_3 films could be deposited with Pr(^{i}PrCp)$_2$(^{i}Pr-amd)/H_2O and Dy(^{i}PrCp)$_2$(^{i}Pr-amd)/O_3 processes but the film growth was not self-limiting.

The same problems with hygroscopicity and carbonate formation as reported in literature were seen also here in the La_2O_3 depositions with water or ozone as the oxygen source. A double oxygen source consisting of H_2O and O_3 pulses separated by purges suppressed hydrogen and carbon levels in the films as measured by TOF-ERDA. It would be interesting to test this approach also for the other rare earth oxides, especially Gd_2O_3 which suffered from rather high carbon contents when deposited with ozone, and hydrogen contents when water was the oxygen source.

Three heteroleptic zirconium precursors were tested for ALD of ZrO_2: Zr(MeCp)(TMEA), Zr(Me_5Cp)(TEA) and Zr(Cp)(^{t}BuDAD)(O^{i}Pr). Zr(Me_5Cp)(TEA) was found to have high thermal stability as self-limiting growth was obtained with the Zr(Me_5Cp)(TEA)/O_3 process at 375 °C with a rate of 0.40 Å/cycle. However, the reactivity of Zr(Me_5Cp)(TEA) towards water was low. Zr(Cp)(^{t}BuDAD)(O^{i}Pr)/O_3 process showed saturation at 250 °C with a growth rate of 0.50 Å/cycle. Saturation was not quite achieved with the Zr(MeCp)(TMEA) precursor with either water or ozone as the oxygen source. Low impurity levels were detected especially with the processes using ozone as the oxygen source.

It has been reported in literature and was also seen in this thesis work that the cubic or tetragonal ZrO_2 phases are often the dominant ones at low deposition temperatures and/or low film thicknesses whereas the monoclinic peaks increase in intensity in XRD with increasing temperature and/or film thickness. Interestingly, with the Zr(Cp)(^{t}BuDAD)(O^{i}Pr)/H_2O process tetragonal films could be deposited at as high temperature as 375 °C with thicknesses of 9 – 70 nm.

9 References

[1] Suntola, T. and Antson, J. US Pat. 4058430 (1977).

[2] Niinistö, L., Ritala, M., Leskelä, M. *Mat. Sci. Eng. B* 41, **1996**, 23.

[3] Ritala, M., Leskelä, M. In Deposition and Processing of Thin Films; Nalwa, H. S., Ed.; Handbook of Thin Film Materials, Vol. 1; Academic Press: San Diego, CA, **2002**; Chapter 2, pp 103−159.

[4] Johnson, R. W., Hultqvist, A., Bent, S. F. Materials Today 17, **2014**, 236 – 246.

[5] Miikkulainen, V., Leskelä, M., Ritala, M., Puurulainen, R. L. *J. Appl. Phys*. 113, **2013**, 021301.

[6] Niinistö, L., Päiväsaari, J. Niinistö, J., Putkonen, M., Nieminen M. Phys. Stat. Sol. A 201, **2004**, 1443.

[7] George, S. M. *Chem. Rev.* 110*,* **2010,** 111.

[8] Ritala, M., Leskelä, M. *J. Phys. IV France* 9, **1999**, Pr8-837.

[9] Elers, K.-E., Blomberg, T., Peussa, M., Aitchison, B., Haukka, S., Marcus, S. *Chem. Vap. Deposition* 12, **2006**, 13.

[10] Elers, K.-E.. Ritala, M., Leskelä, M., Rauhala, E. *Appl. Surf. Sci*. 82/83, **1994**, 468.

[11] Knapas, K., Rahtu, A., Ritala, M. *Chem. Vap. Deposition* 15, **2009**, 269.

[12] Musgrave, C., Gordon, R. *Future Fab Int*. 18, **2005**, 126.

[13] Wiemer, C., Lamagna, L., M Fanciulli, M. *Semicond. Sci. Technol*. 27, **2012**, 074013. REO review

[14] Eisentraut, K. J., Sievers, R. E. *J. Am. Chem. Soc*. 87, **1965**, 5254.

[15] Riha, S. C., Racowski, J. M., Lanci, M. P., Klug, J. A., Hock, A. S., Martinson, A. B. F. *Langmuir* 29, **2013**, 3439.

[16] Ritala, M., Asikainen, T., Leskelä, M. *Electrochem. Solid-State Lett*. 1, **1998**, 156.

[17] Aarik, J., Aidla, A., Mandar, H., Uustare, T., Sammelselg, V. *Thin Solid Films* 408, **2002**, 97.

[18] Kukli, K., Ritala, M., Aarik, J., Uustare, T., Leskelä, M. *J. Appl. Phys*. 92, **2002**, 1833.

[19] Nieminen, M., Putkonen, M., Niinistö, L. *Appl. Surf. Sci*. 174, **2001,** 155.

[20] Nilsen, O., Fjellvag, H. Kjekshus, A. *Thin Solid Films* 450, **2004**, 240.

[21] Niinistö, J., Putkonen, M., Niinistö, L., Arstila, K., Sajavaara, T., Lu, J., Kukli, K., Ritala, M., Leskelä, M. *J. Electrochem. Soc*.153, **2006**, F39.

[22] Abermann, S., Bethge, O., Henkel, C., Bertagnolli, E. *Appl. Phys. Lett*. 94, **2009**, 262904.

[23] Abermann, S., Henkel, C., Bethge, O., Pozzovivo, G., Klang, P. Bertagnolli, E. *Appl. Surf. Sci*. 256, **2010**, 5031.

[24] Jeong, D., Lee, J., Kim, J. *Integrated Ferroelectrics* 67, **2004**, 41.

[25] Cheng, C.-W., Fitzgerald, E. A. *Appl. Phys. Lett*. 93, **2008**, 031902.

[26] Jeona, W.-S., Yang, S., Leeb, C.-S., Kang S.-W. *J. Electrochem. Soc.* 149, **2002**, C306.

[27] Marstell, R. J., Strandwitz, N. C. *J. Appl. Phys*. 118, **2015**, 185304.

[28] Rauwel, E., Clavel, G., Willinger, M.-G., Rauwel, P., Pinna, N. *Angew. Chem. Int. Ed*. 47, **2008**, 3592.

[29] Rauwel, E., Willinger, M.-G., Ducroquet, F., Rauwel, P., Matko, I., Kiselev, D., Pinna, N. *J. Phys. Chem. C* 112*,* **2008**, 12754.

[30] Ritala, M., Kukli, K., Rahtu, A., Räisänen P. I., Leskelä, M., Sajavaara, T., Keinonen, J. *Science,* 288, **2000**, 319.

[31] Xu, L., Fang, G., Caob, Y., Li, A. *Phys. Chem. Chem. Phys*., 18, **2016**, 31223.

[32] Chaukulkar, R. P., Agarwal, S. *J. Vac. Sci. Technol. A*, 31, **2013**, 031509.

[33] Rahtu, A., Ritala, M., Leskelä, M. *Chem. Mater*. 13, **2001**, 1528.

[34] Kim, H., Oh, I.-K. *Jpn. J. Appl. Phys*. 23, **2014**, 03DA01.

[35] Profijt, H. B., Potts, S. E., van de Sanden, M. C. M., Kessels, W. M. M. *J. Vac. Sci. Technol. A* 29, **2011**, 050801.

[36] Scarel, G., Svane, A., Fanciulli, M. *Scientific and Technological Issues Related to Rare Earth Oxides: An Introduction* pp. 3 – 4 in Rare Earth Oxide Thin Films: Growth, Characterization, and Applications, eds. Scarel, G. and Fanciulli, M. (Springer-Verlag Berlin Heidelberg **2007**)

[37] Cotton, S. Lanthanide and Actinide Chemistry, Chapter 2 (John Wiley & Sons, **2006**).

[38] Shannon, R. D. *Acta Cryst. A*. 32, **1976**, 751.

[39] Adachi, G.-Y., Imanaka, N. *Chemical Reviews*, 98, **1998**, 1479.

[40] Jeon, S., Hwang, H. *J. Appl. Phys*. 93, **2003**, 6393.

[41] Zhao, Y., Toyama, M., Kita, K., Kyuno, K., Toriumi, A. Appl. Phys. Lett. 88, **2006,** 072904.

[42] Zhao, Y. *Materials* 5, **2012**, 1413.

[43] Lim, B.S., Rahtu, A., de Rouffignac, P., Gordon, R.G. *Appl. Phys. Lett*. 84, **2004,** 3957.

[44] Kim, S. Y., Kwon, H., Jo, S. J., Ha, J. S., Park, W. T., Kang, D. K., Kim, B.-H. *Appl. Phys. Lett*. 90, **2007**, 103104.

[45] Wang, H., Wang, J.-J., Gordon, R., Lehn, J.-S. M., Li, H., Hong, D., Shenai, D. V. *Electrochem. Solid-State Lett*. 124, **2009**, G13.

[46] Lopes, J. M. J., Roeckerath, M., Heeg, T., Schubert, J., Litmark, U., Mantl, S., Besmehn, A., Myllymäki, P., Niinistö, L., Adamo, C., Schlom, D. G. *ECS Transactions* 11, **2007**, 311.

[47] Jinesh, K. B., Besling, W. F. A., Tois, E., Klootwijk, J. H., Wolters, R., Dekkers, W., Kaiser, M., Bakker, F., Tuominen, M., Roozeboom, F. *Appl. Phys. Lett*. 93, **2008**, 062903.

[48] de Rouffignac, P., Gordon, R. G. *Chem. Vap. Deposition* 12, **2006,** 152.

[49] Hansen, P.-A.; Fjellvåg, H.; Finstad, T.; Nilsen, O. *Dalton Trans*. 42, **2013**, 10778.

[50] Päiväsaari, J., Putkonen, M., Niinistö, L. *Thin Solid Films* 472, **2005,** 275.

[51] Niinistö, J., Petrova, N., Putkonen, M., Niinistö, L., Arstila, K., Sajavaara, T. *J. Crystal Growth* 285, **2005**, 191.

[52] Lu, H. L., Scarel, G., Lamagna, L., Fanciulli, M., Ding, S.-J., Zhang, D. W. *Appl. Phys. Lett.* 93, **2008**, 152906.

[53] Kukli, K., Hatanpää, T., Ritala, M., Leskelä, M. *Chem. Vap. Deposition* 13, **2007,** 546.

[54] Jones, A. C. *J. Mater. Chem*. 12, **2002**, 2576.

[55] Kim, W.-H., Kim, M.-K., Oh, I.-K., Maeng, W. J., Cheon, T., Kim, S.-H., Noori, A., Thompson, D., Chu, S., Kim, H. *J. Am. Ceram. Soc*. 97, **2014**, 1164.

[56] Potter, R. J., Chalker, P. R., Manning, T. D., Aspinall, H. C., Loo, Y. F., Jones, A. C., Smith, L. M., Critchlow, G. W., Schumacher, M. *Chem. Vap. Deposition* 11, **2005**, 159.

[57] Han, J. H., Nyns, L., Delabie, A., Franquet, A., Van Elshocht, S., Adelmann, C. *Chem. Mater*. 26, **2014,** 1404.

[58] Jones, A. C., Aspinall, H. C., Chalker, P. R., Potter, R. J., Kukli, K., Rahtu, A., Ritala, M., Leskelä, M. *J. Mater. Chem.* 14, **2004**, 3101.

[59] Kukli, K. Ritala, M. Pore, V. Leskelä, M. Sajavaara, T. Hegde, R. I. Gilmer, D. C. Tobin, P. J. Jones, A. C., Aspinall, H. C. *Chem. Vap. Deposition* 12, **2006**, 158.

[60] Kukli, K., Ritala, M., Pilvi, T., Sajavaara, T., Leskelä, M., Jones, A. C., Aspinall, H. C., Gilmer, D. C., Tobin, P. J. *Chem. Mater*. 16, **2004,** 5162.

[61] Mai, L., Boysen, N., Subaş, E., de los Arcos, T., Rogalla, D., Grundmeier, G., Bock, C., Hong-Liang Lu, H.-L., Devi, A. *RSC Adv*. 8, **2018**, 4987.

[62] Milanov, A. P., Xu, K., Laha, A., Bugiel, E., Ranjith, R., Schwendt, D., Osten, H. J., Parala, H., Fischer, R. A., Devi, A. *J. Am. Chem. Soc*. 132, **2010,** 36.

[63] Xu, K., Ranjith, R., Laha, A., Parala, H., Milanov, A. P., Fischer, R. A., Bugiel, E., Feydt, J., Irsen, S., Toader, T., Bock, C., Rogalla, D., Osten, H.-J., Kunze, U., Devi, A. *Chem. Mater*. 24, **2012**, 651.

[64] de Rouffignac, P., Yousef, A. P., Kim, K. H., Gordon, R. G. *Electrochem. Solid-State Lett.* 9, **2006**, F45.

[65] de Rouffignac, P., Park, J.-S., Gordon, R. G. *Chem. Mater*. 17, **2005**, 4808.

[66] Putkonen, M., Nieminen, M., Niinistö, J., Sajavaara, T., Niinistö, L. *Chem. Mater*. 13, **2001**, 4701.

[67] Stafford, N. A., Katamreddy, R., Guerin, L., Feist, B., Dussarrat, C., Pallem, V., Weiland, C., Opila, R. *ECS Trans*. 19, **2009**, 525.

[68] L. Nyns, J. G. Lisoni, G. Van den Bosch, S. Van Elshocht, and J. Van Houdt, Phys. Status Solidi A 211, **2014,** 409.

[69] Putkonen, M. Sajavaara, T. Johansson, L.-S. Niinistö L. *Chem. Vap. Dep*. 7, **2001**, 44.

[70] Niinistö, J., Putkonen, M., and Niinistö, L. *Chem. Mater.* 16*,* **2004,** 2953.

[71] Majumder, P., Jursich, G., Kueltzo, A., Takoudis, C. *J. Electrochem. Soc*. 155, **2008**, G152.

[72] Xu, R., Selvaraj, S. K., Azimi, N., Takoudis, C. G. *ECS Trans*. 50, **2013**, 107.

[73] Jo, S. J., Ha, J. S., Park, N. K., Kang, D. K., Kim, B. H. *Thin Solid Films* 513, **2006**, 253.

[74] Tsoutsou, D., Scarel, G., Debernardi, A., Capelli, S. C., Volkos, S. N., Lamagna, L., Schamm, S., Coulon, P. E., Fanciulli, M. *Microelectron. Eng*. 85, **2008,** 2411.

[75] Kim, W.-H., Maeng, W., Moon, K.-J., Myoung, J.-M., Kim, H. *Thin Solid Films* 519, **2010,** 362.

[76] Lee, B., Park, T. J., Hande, A., Kim, M. J., Wallace, R. M., Kim, J., Liu, X., Yi, J. H., Li, H., Rousseau, M., Shenai, D., Suydam, *J. Microelectron. Eng*. 86, **2009,** 1658.

[77] Päiväsaari, J., Putkonen, M., Niinistö, L. *J. Mater. Chem*. 12, **2002**, 1828.

[78] Päiväsaari, J. PhD thesis, Helsinki University of Technology 2006.

[79] Kondo, H., Matsui, H., Furuta, K., Sakashita, M., Zaima, S. *Jap. J. Appl. Phys*. 49, **2010**, 04DA14.

[80] Niinistö, J. PhD thesis Helsinki University of Technology 2006.

[81] Kosola, A., Päiväsaari, J., Putkonen, M., Niinistö, L. *Thin Solid Films* 479, **2005**, 152.

[82] Han, J. H., Delabie, A., Franquet, A., Conard, T., Van Elshocht, S., Adelmann, A. *Chem. Vap. Deposition* 21, **2015**, 352.

[83] Päiväsaari, J., Putkonen, M., Sajavaara, T., Niinistö, L. *J. Alloys Comp*. 374, **2004**, 124.

[84] Päiväsaari, J., Dezelah C. L., Back, D., El-Kaderi, H. M., Heeg, M., Putkonen, M., Niinistö, L., Winter, C. H. *J. Mater. Chem*. 15, **2005,** 4224.

[85] Xu, K. Chaudhuri, A. R., Parala, H., Schwendt, D., de los Arcos, T., Osten H. J., Devi A. *J. Mater. Chem. C*, 1, **2013**, 3939.

[86] Litta, E. D., Hellström, P.-E., Henkel, C., Valerio, S., Hallén, A., Östling, M. *J. Electrochem. Soc*. 160, **2013,** D538.

[87] Bosund, M., Mizohata, K., Hakkarainen, T., Putkonen, M., Söderlund, M., Honkanen, S., Lipsanen, H. *Appl. Surf. Sci*. 256, **2009,** 847.

[88] Adelmann, C., Swerts, J., Conard, T., Brijs, B., Franquet, A., Hardy, A., Tielens, H., Opsomer, K., Moussa, A., Van Bael, M. K., Jurczak, M., Kittl, J. A., Van Elshocht S. *ECS Transactions*, 34, **2011**, 473.

[89] Nyns, L., Shi, X., Tielens, H., Van Elshocht S., Date L., Schreutelkamp R. *J. Vac. Sci. Technol. A* 30, **2012**, 01A120.

[90] Rahman, R., Klesko, J. P., Dangerfield, A., Fang, M., Lehn, J.-S. M., Dezelah, C. L., Kanjolia, R. K., Chabal, Y. J. *J. Vac. Sci. Technol. A* 37, **2019**, 011504.

[91] Rahman, R., Klesko, J. P., Dangerfield, A., Mattson, E. C., Chabal, Y. J. *ACS Appl. Mater. Interfaces* 10, **2018**, 32818.

[92] Blanquart, T., Kaipio, M., Niinistö, J., Gavagnin, M., Longo, V., Blanquart, L., Lansalot, C., Noh, W., Wanzenböck, H. D., Ritala, M., Leskelä M. *Chem. Vap. Deposition* 20, **2014**, 217.

[93] Oh, I.-K., Kim, K., Lee, Z., Ko, K. Y., Lee, C.-W., Lee, S. J., Myung, J. M., Lansalot-Matras, C., Noh, W., Dussarrat, C., Kim, H., Lee, H.-B.-R. *Chem. Mater*. 27, **2015**, 148.

[94] Päiväsaari, J., Niinistö, J., Arstila, K., Kukli, K., Putkonen, M., Niinistö, L. *Chem. Vap. Deposition* 11, **2005,** 415.

[95] Xu, R., Tao, Q., Yang, Y., Takoudis C. G. *Appl. Surf. Sci*. 258, **2012**, 8514.

[96] Scarel, G., Bonera, E., Wiemer, C., Tallarida, G., Spiga, S., Fanciulli, M., Fedushkin, I. L., Schumann, H., Lebedinskii, Y., Zenkevich, A. *Appl. Phys. Lett*. 85, **2004,** 630.

[97] Park, I.-S., Jung, Y. C., Seong, S., Ahn, J., Kang, J., Noh W., Lansalot-Matras, C. *J. Mater. Chem. C*, 2, **2014**, 9240.

[98] Lee, J.-S., Kim, W.-H., Oh, I.-K., Kim, M.-K., Lee, G., Lee, C.-W., Park, J., Lansalot-Matras, C., Noh, W., Kim, H. *Appl. Surf. Sci*. 297, **2014**, 16.

[99] Navrotsky, A. *J. Mater. Chem*. 15, **2005,** 1883.

[100] Yashima, M., Kakihana, M., Yoshimura, M. *Solid State Ionics* 86-88, **1996**, 1131.

[101] Lamperti, A., Lamagna, L., Congedo, G., Spiga S. *J. Electrochem. Soc*. 158, **2011**, G221.

[102] Robertson, J. *J. Vac. Sci. Technol. B* 18, **2000**, 1785.

[103] Kim S. K., Hwang, C. S. *Electrochem. Solid-State Lett*. 11, **2008**, G9.

[104] Kärkkänen, I., Shkabko, A., Heikkilä, M., Niinistö, J., Ritala, M., Leskelä, M., Hoffmann-Eifert, S., Waser, R. *Phys. Status Solidi A* 211, **2014**, 301.

[105] Ritala, M., Leskelä, M. *Appl. Surf. Sci.* 75, **1994**, 333.

[106] Kukli, K., Forsgren, K., Aarik, J., Uustare, T., Aidla, A., Niskanen, A., Ritala, M., Leskelä, M., Hårsta, A. *J. Crystal Growth* 231, **2001**, 262.

[107] Forsgren, K., Westlinder, J., Lu, J., Olsson, J., Hårsta, A. *Chem. Vap. Deposition* 8, **2002**, 105.

[108] Putkonen, M., Niinistö, L. *J. Mater. Chem*. 11, **2001**, 3141.

[109] Lee, B., Choi, K. J., Hande, A., Kim, M. J., Wallace, R. M., Kim, J., Senzaki, Y., Shenai, D., Li, H., Rousseau, M., Suydam, *J. Microelectron. Eng*. 86, **2009**, 272.

[110] Kukli, K., Ritala, M., Leskelä, M. *Chem. Vap. Deposition* 6, **2000**, 297.

[111] Hausmann, D. M., Kim, E., Becker, J., Gordon, R. G. *Chem. Mater*. 14, **2002**, 4350.

[112] Kim, S. K., Hwang, C. S. *Electrochem. Solid-State Lett*. 113, **2008**, G9.

[113] Triyoso, D. H., Gregory, R., Park, M., Wang, K., Lee, S. I. *J. Electrochem. Soc*. 155, **2008**, H43.

[114] Niinistö, J., Kukli, K., Kariniemi, M., Ritala, M., Leskelä, M., Blasco, N., Pinchart, A., Lachaud, C., Laaroussi, N., Wang, Z., Dussarrat, C. *J. Mater. Chem*. 18, **2008**, 5243.

[115] Clark, R. D., Consiglio, S., Wajda, C. S., Leusink, G. J., Sugawara, T., Nakabayashi, H., Jagannathan, H., Edge, L. F., Jamison, P., Paruchuri, V. K., Iijima, R., Takayanagi, M., Linder, B. P., Bruley, J., Copel, M., Narayanan, V. *ECS Transactions* 16, **2008**, 291.

[116] Putkonen, M., Niinistö, J., Kukli, K., Sajavaara, T., Karppinen, M., Yamauchi, H., Niinistö, L. *Chem. Vap. Deposition* 9, **2003**, 207.

[117] Dezelah, C., Niinistö, J., Kukli, K., Munnik, F., Lu, J., Ritala, M., Leskelä, M., Niinistö, L. *Chem. Vap. Deposition* 14, **2008**, 358.

[118] Niinistö, J., Kukli, K., Tamm, A., Putkonen, M., Dezelah, C. L., Niinistö, L., Lu, J., Song, F., Williams, P., Heys, P. N., Ritala, M., Leskelä, M. *J. Mater. Chem*. 18, **2008**, 3385.

[119] Niinistö, J., Hatanpää, T., Kariniemi, M., Mäntymäki, M., Costelle, L., Mizohata, K., Kukli, K., Ritala, M., Leskelä, M. *Chem. Mater*. 24, **2012**, 2002.

[120] Black, K., Aspinall, H. C., Jones, A. C., Przybylak, K., Bacsa, J., Chalker, P. R., Taylor, S., Zhao, C. Z., Elliott, S. D., Zydordand, A., Heys, P. N. *J. Mater. Chem*. 18, **2008**, 4561.

[121] Gaskell, J.M., Jones, A. C., Black, K., Chalker, P. R., Leese, T., Kingsley, A., Odedra, R., Heys, P. N., *Surf. Coat. Technol*. 201, **2007**, 9095.

[122] Matero, R., Ritala, M., Leskelä, M., Sajavaara, T., Jones, A. C., Roberts, J. L. *Chem. Mater*. 16, **2004**, 5630.

[123] Matero R., Ritala, M., Leskelä, M., Jones, A. C., Williams, P. A., Bickley, J. F., Steiner, A., Leedham, T.J., Davies H.O. *J. Non-Crystal. Solids* 303, **2002**, 24.

[124] Nam, W.-H., Rhee, S.-W. *Chem. Vap. Deposition* 10, **2004**, 201.

[125] Blanquart, T., Niinistö, J., Aslam, N., Banerjee, M., Tomczak, Y., Gavagnin, M., Longo, V., Puukilainen, E., Wanzenboeck, H. D., Kessels, W. M. M., Devi, A., Hoffmann-Eifert, S., Ritala, M., Leskelä, M. *Chem. Mater*. 25, **2013**, 3088.

[126] Kaipio, M., Blanquart, T., Banerjee, M., Xu, K., Niinistö, J., Longo, V., Mizohata, K., Devi, A., Ritala, M., Leskelä, M. *Chem. Vap. Deposition* 20, **2014**, 209.

[127] Leskelä, M., Kukli, K., Ritala, M. *J. Alloys Comp*. 418, **2006**, 27.

[128] Moore, G. *Electronics* 38, **1965**, 114.

[129] Osten, H. J., Laha, A., Czernohorsky, M., Bugiel, E., Dargis, R., Fissel, A. *Phys. Stat. Sol. A* 205, **2008**, 695.

[130] Packan, P. A. *Science* 285, **1999**, 2079.

[131] Mistry, K., Allen, C., Auth, C., Beattie, B., Bergstrom, D., Bost, M., Brazier, M., Buehler, M., Cappellani, A., Chau, R., Choi, C.-H., Ding, G., Fischer, K., Ghani, T., Grover, R., Han, W., Hanken, D., Hattendorf, M., He, J., Hicks, J., Huessner, R., Ingerly, D., Jain, P., James, R., Jong, L., Joshi, S., Kenyon, C., Kuhn, K., Lee, K., Liu, H., Maiz, J., McIntyre, B., Moon, P., Neirynck, J., Pae, S., Parker, C., Parsons, D., Prasad, C., Pipes, L., Prince, M., Ranade, P., Reynolds, T., Sandford, J., Shifren, L., Sebastian, J., Seiple, J., Simon, D., Sivakumar, S., Smith, P., Thomas, C., Troeger, T., Vandervoorn, P., Williams,

S., Zawadzki, K. *Proc. International Electron Devices Meeting 2007*, IEDM Tech. Dig. **2007**, 247.

[132] Ono, H., Katsumata, T. *Appl. Phys. Lett*. 78, **2001**, 1832.

[133] Lamagna, L., Wiemer, C. Perego, M. Volkos, S. N. Baldovino, S. Tsoutsou D., Schamm-Chardon, S. Coulon, P. E., Fanciulli, M., *J. Appl. Phys*. 108, **2010,** 084108.

[134] Fischetti, M. V., Neumayer, D. A., Cartier, E. A. *J. Appl. Phys*. 90, **2001**, 4587.

[135] Liu, Y., Xu, M., Heo, J., Ye, P. D., Gordon, R. G. *Appl. Phys. Lett*. 97, **2010**, 162910.

[136] Myllymäki, P., Roeckerath, M., Marcelo Lopes, J., Schubert, J., Mizohata, K., Putkonen, M., Niinistö, L. *J. Mater. Chem*. 20, **2010**, 4207.

[137] Myllymäki, P., Roeckerath, M., Putkonen, M., Lenk, S.,Schubert, J., Niinistö, L., Mantl, S. *Appl. Phys. A* 88, **2007**, 633.

[138] Myllymäki, P., Nieminen, M., Niinistö, J., Putkonen, M., Kukli, K., Niinistö, L. *J. Mater. Chem.* 16, **2006**, 563.

[139] Wiemer, C., Lamagna, L., Baldovino, S., Perego, M., Schamm-Chardon, S., Coulon, P.-E., Salicio, O., Congedo, G., Spiga, S., Fanciulli, M. *Appl. Phys. Lett*. 96, **2010**, 182901.

[140] Bang, S., Lee, S., Jeon, S., Kwon, S., Jeong, W., Kim S., Jeon, H. *J. Electrochem. Soc.* 155, **2008**, H633.

[141] Triyoso, D. H., Hegde, R. I., Schaeffer, J. K., Gregory, R., Wang, X.-D., Canonico, M., Roan, D., Hebert, E. A., Kim, K., Jiang, J., Rai, R., Kaushik, V., Samavedam, S. B. J. Vac. Sci. Tech. B 25, **2007**, 845.

[142] Kim, S. K., Popovici, M. *MRS Bulletin* 43, **2018**, 334.

[143] Park, B.-E., Oh, I.-K., Mahata, C., Lee, C. W., Thompson, D., Lee, H.-B.-R., Maeng, W. J., Kim, H. *J. Alloys Comp*. 722, **2017**, 307.

[144] Wu, Y.-H., Kao, C.-K., Chen, B.-Y., Lin, Y.-S., Li, M.-Y., Wu, H.-C. *Appl. Phys. Lett*. 93, **2008**, 033511.

[145] Cho, H. J., Kim, Y. D., Park, D. S., Lee, E., Park, C. H., Jang, J. S., Lee, K. B., Kim, H. W., Ki, Y. J., Han, I. K., Song, Y. W. *Solid-State Electron*. 51, **2007**, 1529.

[146] International Technology Roadmap for Semiconductors (2013), http://www.itrs2.net.

[147] Chen, H.-Y., Brivio, S., Chang, C.-C., Frascaroli, J., Hou, T.-H., Hudec, B., Liu, M., Lv H., Molas, G., Sohn, J., Spiga, S., Teja, V. M., Vianello, E., Wong H.-S. P. *J. Electroceram*. 39, **2017**, 21.

[148] Balatti, S., Larentis, S., Gilmer, D. C., Ielmini, D. *Adv. Mater*. 25, **2013**, 1474.

[149] Steele, B. C. H., Heinzel, A. *Nature* 414, **2001**, 345.

[150] Minh, N. Q. *Solid State Ionics* 174, **2004**, 271.

[151] Jacobson, A. J. *Chem. Mater*. 22, **2010**, 660.

[152] Will, J., Mitterdorfer, A., Kleinlogel, C., Perednis, D., Gauckler, L. J. *Solid State Ionics* 131, **2000**, 79.

[153] Zhao, F., Virkar, A. V. *J Power Sources* 141, **2005**, 79

[154] Arachi, Y., Sakai, H., Yamamoto, O., Takeda, Y., Imanishai, N. *Solid State Ionics* 121, **1999**, 133.

[155] Cassir, M., Ringuedé, A. Niinistö, L. *J. Mater. Chem*. 20, **2010**, 8987.

[156] Ji, S., Chang, I., Lee, Y. H., Park, J., Paek, J. Y., Lee, M. H., Cha, S. W. *Nanoscale Res. Lett.* 8, **2013**, 48.

[157] de Souza, S., Visco, S. J., de Jonghe, L. C. *Solid State Ionics* 98, **1997**, 57.

[158] Asundi, A. S., Raiford, J. A., Bent, S. F. *ACS Energy Lett*. 4, **2019**, 908.

[159] Park, J., Lee, Y., Chang, I., Cho, G. Y., Ji, S., Lee, W., Cha, S. W. *Energy* 116, **2016**, 170.

[160] Gong, Y., Patel, R. L., Liang, X., Palacio, D., Song, X., Goodenough, J. B., Huang, K. *Chem. Mater*. 25, **2013**, 4224.

[161] Keuter, T., Mauer, G., Vondahlen, F., Iskandar, R., Menzler, N. H., Vaßen, R. *Surf. Coat. Technol*. 288, **2016**, 211.

[162] Kostestkyy, P., Yu, J., Gorte, R. J., Mpourmpakis, G. *Cat. Sci. Technol*. 4, **2014,** 3861.

[163] Rosynek, M. P., Koprowski, R. J., Dellisante, G. N. *J. Catal.* 122, **1990**, 80.